Yukawa textures and charged Higgs boson phenomenology in the type-III two-Higgs-doublet model

J. L. Díaz-Cruz,[1,*] J. Hernández-Sánchez,[2,†] S. Moretti,[3,‡] R. Noriega-Papaqui,[4,§] and A. Rosado[5,‖]

[1]*Facultad de Ciencias Físico-Matemáticas, BUAP, Apartado Postal 1364, C.P. 72000 Puebla, Puebla, México, and Dual C-P Institute of High Energy Physics, México*

[2]*Facultad de Ciencias de la Electrónica, BUAP, Avenida San Claudio y 18 Sur, C.P. 72500 Puebla, Puebla, México, and Dual C-P Institute of High Energy Physics, México*

[3]*School of Physics and Astronomy, University of Southampton, Highfield, Southampton SO17 1BJ, United Kingdom*

[4]*Centro de Investigación en Matemáticas, Universidad Autónoma del Estado de Hidalgo, Carretera Pachuca-Tulancingo Km. 4.5, C.P. 42184, Pachuca, Hidalgo, México, and Dual C-P Institute of High Energy Physics, México*

[5]*Instituto de Física, BUAP, Apartado Postal J-48, C.P. 72570 Puebla, Puebla, México*

(Received 3 March 2009; published 29 May 2009)

We discuss the implications of assuming a four-zero Yukawa texture for the properties of the charged Higgs boson within the context of the general two-Higgs-doublet model of type III. We begin by presenting a detailed analysis of the charged Higgs boson couplings with heavy quarks and the resulting pattern for its decays. The production of charged Higgs bosons is also sensitive to the modifications of its couplings, so that we also evaluate the resulting effects on the top decay $t \to bH^+$ as well as on "direct" $c\bar{b} \to H^+ + \text{c.c.}$ and "indirect" $q\bar{q}, gg \to \bar{t}bH^+ + \text{c.c.}$ production. A significant scope exists at the Large Hadron Collider for several $H^\pm$ production and decay channels combined to enable one to distinguish between such a model and alternative two-Higgs-doublet scenarios.

DOI: 10.1103/PhysRevD.79.095025 PACS numbers: 12.60.Cn, 12.60.Fr, 11.30.Er

I. INTRODUCTION

Detecting a charged Higgs boson during the imminent Large Hadron Collider (LHC) experimental running would constitute clear evidence of physics beyond the standard model (SM) [1]. Charged Higgs bosons appear in many well motivated extensions of the SM, whose phenomenology has been widely studied over the years [2–4]. In particular, two-Higgs-doublet models (2HDMs), in both supersymmetry (SUSY) and non-SUSY versions [5,6], can be considered as a prototype of a Higgs sector that includes a charged Higgs boson ($H^\pm$). It is expected that the LHC will allow us to test the mechanism of electroweak symmetry breaking (EWSB) and, in particular, to probe the properties of charged Higgs bosons, which represent a unique probe of a weakly interacting theory, as is the case of the minimal supersymmetric standard model (MSSM) [5] and general 2HDMs of type I, II, III, and IV (2HDM-I, 2HDM-I, 2HDM-III, and 2HDM-IV) [7], or whether strongly interacting scenarios are instead realized, like in the old technicolor models or similar ones discussed more recently [8]. Ultimately, while many analyses in this direction can be carried out at the LHC, it will be a future International Linear Collider (ILC) [9] or Compact Linear Collider (CLIC) [10] which will have the definite word about exactly which mechanism of mass generation and which realization of it occurs in nature.

The 2HDM-II has been quite attractive to date, in part because it coincides with the Higgs sector of the MSSM, wherein each Higgs doublet couples to the u- or d-type fermions separately.[1] However, this is valid only at tree level [12]. When radiative effects are included, it turns out that the MSSM Higgs sector corresponds to the most general version of the 2HDM, namely, the 2HDM-III, whereby both Higgs fields couple to both quarks and leptons. Thus, we can consider the 2HDM-III as a generic description of physics at a higher scale (of order TeV or maybe even higher), whose low-energy imprints are reflected in the Yukawa coupling structure. With this idea in mind, some of us have presented a detailed study of the 2HDM-III Yukawa Lagrangian [13], under the assumption of a specific texture pattern [14], which generalizes the original model of Ref. [15]. Phenomenological implications of this model for the neutral Higgs sector, including lepton flavor violation and/or flavor changing neutral currents have been presented in a previous work [16]. Here we are interested in extending such an approach to investigate charged Higgs boson phenomenology: Namely, we want to study the implications of this Yukawa texture for the charged Higgs boson properties (masses and couplings) and discuss in detail the resulting pattern of charged Higgs boson decays and main production reactions at the LHC.

Decays of charged Higgs bosons have been studied in the literature, including the radiative modes $W^\pm\gamma$ and

*jldiaz@fcfm.buap.mx
†jaimeh@ece.buap.mx
‡stefano@soton.ac.uk
§rnoriega@uaeh.edu.mx
‖rosado@sirio.ifuap.buap.mx

[1]Notice that there exist significant differences between the 2HDM-II and MSSM though, when it comes to their mass/coupling configurations and possible Higgs signals [11].

$W^{\pm}Z^0$ [17], mostly within the context of the 2HDM-II or its SUSY incarnation (i.e., the MSSM) but also by using an effective Lagrangian extension of the 2HDM [18] and, more recently, within an extension of the MSSM with one complex Higgs triplet (MSSM + 1CHT) [19,20]. Charged Higgs boson production at hadron colliders was studied long ago [21], and, more recently, systematic calculations of production processes at the LHC have been presented [22].

Current bounds on the mass of a charged Higgs boson have been obtained at the Tevatron, by studying the top decay $t \to bH^+$, which already eliminates large regions of the parameter space [23], whereas LEP2 bounds imply that, approximately, $m_{H^+} > 80$ GeV [24,25], rather model independently. Concerning theoretical limits, tree-level unitarity bounds on the 2HDM Higgs masses have been studied in generic 2HDMs, and, in particular, an upper limit for the charged Higgs mass of 800 GeV or so can be obtained, according to the results of Ref. [26].

This paper is organized as follows. In Sec. II, we discuss the Higgs-Yukawa sector of the 2HDM-III; in particular, we derive the expressions for the charged Higgs boson couplings to heavy fermions. Then, in Sec. III, we derive the expressions for the decays $H^+ \to f_i \bar{f}_j$, and numerical results are presented for some 2HDM-III scenarios, defined for phenomenological purposes. A discussion of the main production mechanisms at the LHC is presented in Sec. IV. These include the top decay $t \to bH^+$ as well as s-channel production of charged Higgs bosons through $c\bar{b}(\bar{c}b)$ fusion [27] and the multibody more $q\bar{q}, gg \to t\bar{b}H^- + \text{c.c.}$ (charge conjugated). These mechanisms depend crucially on the parameters of the underlying model, and large deviations should be expected in the 2HDM-III with respect to the 2HDM-II. Actual LHC event rates are given in Sec. V. Finally, we summarize our results and present the conclusions in Sec. VI. Notice that in carrying out this plan, unlike other references [28,29], where the 2HDM-II and the 2HDM-III appear as different structures, we shall consider here that, under certain limits, the 2HDM-III reduces to the 2HDM-II and, therefore, that the properties of the charged Higgs bosons change continuously from one model to the other.

II. THE CHARGED HIGGS BOSON LAGRANGIAN AND THE FERMIONIC COUPLINGS

We shall follow Refs. [13,16], where a specific four-zero texture has been implemented for the Yukawa matrices within the 2HDM-III. This allows one to express the couplings of the neutral and charged Higgs bosons in terms of the fermion masses, Cabibbo-Kobayashi-Maskawa (CKM) mixing angles, and certain dimensionless parameters, which are to be bounded by current experimental constraints. Thus, in order to derive the interactions of the charged Higgs boson, the Yukawa Lagrangian is written as follows:

$$\mathcal{L}_Y = Y_1^u \bar{Q}_L \tilde{\Phi}_1 u_R + Y_2^u \bar{Q}_L \tilde{\Phi}_2 u_R + Y_1^d \bar{Q}_L \Phi_1 d_R + Y_2^d \bar{Q}_L \Phi_2 d_R, \tag{1}$$

where $\Phi_{1,2} = (\phi^+_{1,2}, \phi^0_{1,2})^T$ refer to the two Higgs doublets, $\tilde{\Phi}_{1,2} = i\sigma_2 \Phi^*_{1,2}$, Q_L denotes the left-handed fermion doublet, u_R and d_R are the right-handed fermions singlets, and, finally, $Y^{u,d}_{1,2}$ denote the (3×3) Yukawa matrices. Similarly, one can write the corresponding Lagrangian for leptons.

After spontaneous EWSB and including the diagonalizing matrices for quarks and Higgs bosons,[2] the interactions of the charge Higgs boson H^+ with quark pairs acquire the following form:

$$\mathcal{L}^{\bar{q}_i q_j H^+} = \frac{g}{2\sqrt{2}M_W} \sum_{l=1}^{3} \bar{u}_i \Big\{ (V_{\rm CKM})_{il} \Big[\tan\beta m_{d_l} \delta_{lj} - \sec\beta \Big(\frac{\sqrt{2}M_W}{g} \Big) (\tilde{Y}_2^d)_{lj} \Big] + \Big[\cot\beta m_{u_i} \delta_{il} - \csc\beta \Big(\frac{\sqrt{2}M_W}{g} \Big) (\tilde{Y}_1^u)^\dagger_{il} \Big] (V_{\rm CKM})_{lj} + (V_{\rm CKM})_{il} \Big[\tan\beta m_{d_l} \delta_{lj} - \sec\beta \Big(\frac{\sqrt{2}M_W}{g} \Big) (\tilde{Y}_2^d)_{lj} \Big] \gamma^5 - \Big[\cot\beta m_{u_i} \delta_{il} - \csc\beta \Big(\frac{\sqrt{2}M_W}{g} \Big) (\tilde{Y}_1^u)^\dagger_{il} \Big] (V_{\rm CKM})_{lj} \gamma^5 \Big\} d_j H^+, \tag{2}$$

where $V_{\rm CKM}$ denotes the mixing matrices of the quark sector (and similarly for the leptons). The term proportional to δ_{ij} corresponds to the contribution that would arise within the 2HDM-II, while the terms proportional to $\tilde{Y}_2^d$ and $\tilde{Y}_1^u$ denote the new contributions from the 2HDM-III. These contributions depend on the rotated matrices: $\tilde{Y}_n^q = O_q^T P_q Y_n^q P_q^\dagger O_q$ ($n = 1$ when $q = u$, and $n = 2$ when $q = d$), where O_q is the diagonalizing matrix, while P_q includes the phases of the Yukawa matrix. In order to evaluate $\tilde{Y}_n^q$, we shall consider that all Yukawa matrices have the Hermitian four-zero texture form [14], and the quark masses have the same form, which are given by

$$M^q = \begin{pmatrix} 0 & C_q & 0 \\ C_q^* & \tilde{B}_q & B_q \\ 0 & B_q^* & A_q \end{pmatrix} \qquad (q = u, d). \tag{3}$$

This is called a four-zero texture because one assumes that the Yukawa matrices are Hermitian; therefore, each u- and d-type Yukawa matrix contains two independent zeros.

[2]The details of both diagonalizations are presented in Ref. [13]

According to current analyses, this type of texture satisfies the experimental constraints and at the same time it permits one to derive analytical expressions for the Higgs boson fermion couplings.

To diagonalize M^q, we use the matrices O_q and P_q, in the following way [14]:

$$\bar{M}^q = O_q^T P_q M^q P_q^\dagger O_q. \tag{4}$$

Then one can derive a better approximation for the product $O_q^T P_q Y_n^q P_q^\dagger O_q$, expressing the rotated matrix $\tilde{Y}_n^q$, in the form

$$[\tilde{Y}_n^q]_{ij} = \frac{\sqrt{m_i^q m_j^q}}{v}[\tilde{\chi}_n^q]_{ij} = \frac{\sqrt{m_i^q m_j^q}}{v}[\chi_n^q]_{ij} e^{i\vartheta_{ij}^q}. \tag{5}$$

In order to perform our phenomenological study, we find it convenient to rewrite the Lagrangian given in Eq. (2) in terms of the coefficients $[\tilde{\chi}_n^q]_{ij}$, as follows:

$$\begin{aligned}\mathcal{L}^q = & \frac{g}{2\sqrt{2}M_W}\sum_{l=1}^{3}\bar{u}_i\Bigg\{(V_{\mathrm{CKM}})_{il} \\ & \times\left[\tan\beta m_{d_l}\delta_{lj} - \frac{\sec\beta}{\sqrt{2}}\sqrt{m_{d_l}m_{d_j}}\tilde{\chi}_{lj}^d\right] \\ & + \left[\cot\beta m_{u_i}\delta_{il} - \frac{\csc\beta}{\sqrt{2}}\sqrt{m_{u_i}m_{u_l}}\tilde{\chi}_{il}^u\right](V_{\mathrm{CKM}})_{lj} \\ & + (V_{\mathrm{CKM}})_{il}\left[\tan\beta m_{d_l}\delta_{lj} - \frac{\sec\beta}{\sqrt{2}}\sqrt{m_{d_l}m_{d_j}}\tilde{\chi}_{lj}^d\right]\gamma^5 \\ & - \left[\cot\beta m_{u_i}\delta_{il} - \frac{\csc\beta}{\sqrt{2}}\sqrt{m_{u_i}m_{u_l}}\tilde{\chi}_{il}^u\right](V_{\mathrm{CKM}})_{lj}\gamma^5\Bigg\}d_j H^+,\end{aligned} \tag{6}$$

where we have redefined $[\tilde{\chi}_1^u]_{ij} = \tilde{\chi}_{ij}^u$ and $[\tilde{\chi}_2^d]_{ij} = \tilde{\chi}_{ij}^d$. Then, from Eq. (6), the couplings $\bar{u}_i d_j H^+$ and $u_i \bar{d}_j H^-$ are given by

$$\begin{aligned} g_{H^+\bar{u}_i d_j} &= -\frac{ig}{2\sqrt{2}M_W}(S_{ij} + P_{ij}\gamma_5), \\ g_{H^- u_i \bar{d}_j} &= -\frac{ig}{2\sqrt{2}M_W}(S_{ij} - P_{ij}\gamma_5), \end{aligned} \tag{7}$$

where S_{ij} and P_{ij} are defined as

$$\begin{aligned} S_{ij} = & \sum_{l=1}^{3}(V_{\mathrm{CKM}})_{il}\left[\tan\beta m_{d_l}\delta_{lj} - \frac{\sec\beta}{\sqrt{2}}\sqrt{m_{d_l}m_{d_j}}\tilde{\chi}_{lj}^d\right] \\ & + \left[\cot\beta m_{u_i}\delta_{il} - \frac{\csc\beta}{\sqrt{2}}\sqrt{m_{u_i}m_{u_l}}\tilde{\chi}_{il}^u\right](V_{\mathrm{CKM}})_{lj}, \\ P_{ij} = & \sum_{l=1}^{3}(V_{\mathrm{CKM}})_{il}\left[\tan\beta m_{d_l}\delta_{lj} - \frac{\sec\beta}{\sqrt{2}}\sqrt{m_{d_l}m_{d_j}}\tilde{\chi}_{lj}^d\right] \\ & - \left[\cot\beta m_{u_i}\delta_{il} - \frac{\csc\beta}{\sqrt{2}}\sqrt{m_{u_i}m_{u_l}}\tilde{\chi}_{il}^u\right](V_{\mathrm{CKM}})_{lj}. \end{aligned} \tag{8}$$

As it was discussed in Ref. [13], most low-energy processes imply weak bounds on the coefficients $\tilde{\chi}_{ij}^q$, which turn out to be of $O(1)$. However, some important constraints on $\tan\beta$ have started to appear, based on B physics [30]. In order to discuss these results, we find it convenient to generalize the notation of Ref. [31] and define the couplings $\bar{u}_i d_j H^+$ and $u_i \bar{d}_j H^-$ in terms of the matrices X_{ij}, Y_{ij} and Z_{ij} (for leptons). In our case these matrices are given by

$$\begin{aligned} X_{lj} &= \left[\tan\beta\delta_{lj} - \frac{\sec\beta}{\sqrt{2}}\sqrt{\frac{m_{d_j}}{m_{d_l}}}\tilde{\chi}_{lj}^d\right], \\ Y_{il} &= \left[\cot\beta\delta_{il} - \frac{\csc\beta}{\sqrt{2}}\sqrt{\frac{m_{u_l}}{m_{u_i}}}\tilde{\chi}_{il}^u\right], \end{aligned} \tag{9}$$

where X_{lj} and Y_{il} are related with S_{ij} and P_{ij} defined in the Eq. (8) as follows:

$$\begin{aligned} S_{ij} &= \sum_{l=1}^{3}[(V_{\mathrm{CKM}})_{il}m_{d_l}X_{lj} + m_{u_i}Y_{il}(V_{\mathrm{CKM}})_{lj}], \\ P_{ij} &= \sum_{l=1}^{3}[(V_{\mathrm{CKM}})_{il}m_{d_l}X_{lj} - m_{u_i}Y_{il}(V_{\mathrm{CKM}})_{lj}]. \end{aligned} \tag{10}$$

The 33 elements of these matrices reduce to the expressions for the parameters X, Y, and Z ($= X_{33}$, Y_{33}, Z_{33}) used in Ref. [31]. Based on the analysis of $B \to X_s\gamma$ [31,32], it is claimed that $X \leq 20$ and $Y \leq 1.7$ for $m_{H^+} > 250$ GeV, while for a lighter charged Higgs boson mass $m_{H^+} \sim 200$ GeV, one gets $(X, Y) \leq (18, 0.5)$. Figure 1 shows the values of (X, Y) as a function of $\tan\beta$ within our model. Thus, we find important bounds: $|\chi_{33}^{u,d}| \lesssim 1$ for $0.1 < \tan\beta \leq 70$. Although in our model there are additional contributions (for instance, from c quarks, which are proportional to X_{23}), they are not relevant because the Wilson coefficients in the analysis of $B \to X_s\gamma$ are functions of m_c^2/M_W^2 or $m_c^2/m_{H^+}^2$ [33], that is, negligible when compared to the leading X_{33} effects, whose Wilson coefficients depend on m_t^2/M_W^2 or $m_t^2/m_{H^+}^2$. Other constraints on the charged Higgs mass and $\tan\beta$, based on Δa_μ, the ρ parameter, as well as B decays into the tau lepton, can be obtained [34,35]. For instance, as can be read from Ref. [36], one has that the decay $B \to \tau\nu$ implies a constraint such that, for $m_{H^+} = 200$ (300) GeV, values of $\tan\beta$ less than about 30 (50) are still allowed, within MSSM or 2HDM-III: However, these constraints can only be taken as estimates, as it is likely that they would be modified for 2HDM-III. In summary, we find that low-energy constraints still allow one to have $\tilde{\chi}_{ij}^q = O(1)$.[3]

[3]A more detailed analysis that includes the most recent data is underway [37]

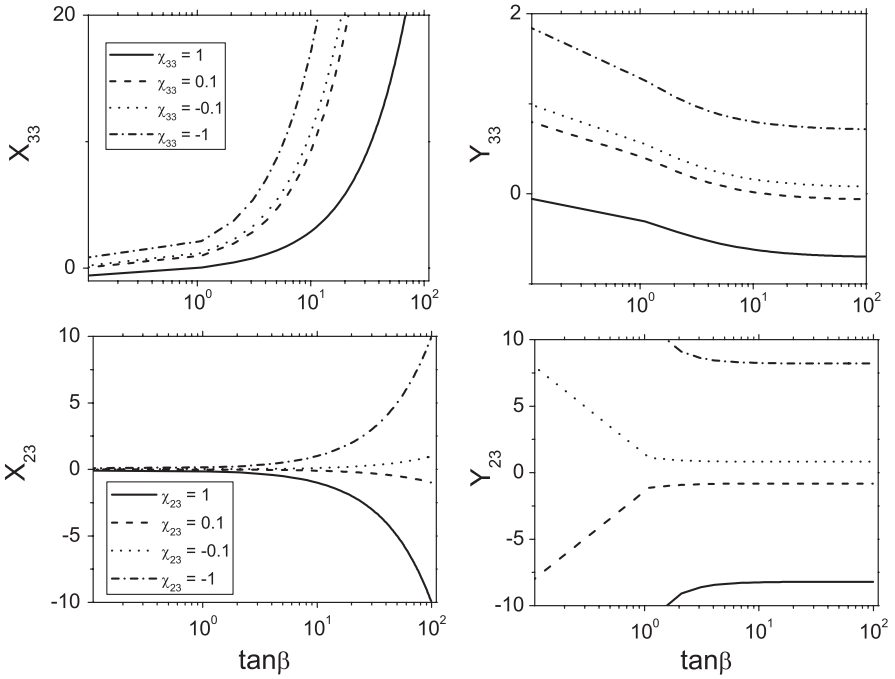

FIG. 1. The figure shows X_{33}, Y_{33}, X_{23}, and Y_{23} vs $\tan\beta$, taking $\tilde{\chi}^{u,d}_{3,3} = 1$ (solid line), $\tilde{\chi}^{u,d}_{3,3} = 0.1$ (dashed line), $\tilde{\chi}^{u,d}_{3,3} = -0.1$ (dotted line), and $\tilde{\chi}^{u,d}_{3,3} = -1$ (dashed-dotted line).

III. DECAYS OF THE CHARGED HIGGS BOSON

Let us now discuss the decay modes of the charged Higgs boson within our model. Hereafter, we shall refer to four benchmark scenarios, namely: (i) *scenario A*: $\tilde{\chi}^u_{ij} = 1$, $\tilde{\chi}^d_{ij} = 1$; (ii) *scenario B*: $\tilde{\chi}^u_{ij} = 0.1$, $\tilde{\chi}^d_{ij} = 1$; (iii) *scenario C*: $\tilde{\chi}^u_{ij} = 1$, $\tilde{\chi}^d_{ij} = 0.1$; (iv) *scenario D*: $\tilde{\chi}^u_{ij} = 0.1$, $\tilde{\chi}^d_{ij} = 0.1$. We have performed the numerical analysis of charged Higgs boson decays by taking $\tan\beta = 0.1, 1, 15, 70$ and varying the charged Higgs boson mass within the interval 100 GeV $\leq m_{H^\pm} \leq$ 1000 GeV, further fixing $m_{h^0} = 120$ GeV, $m_{A^0} = 300$ GeV, and the mixing angle at $\alpha = \pi/2$.

The condition $\frac{\Gamma_{H^+}}{m_{H^+}} < \frac{1}{2}$ in the frame of the 2HDM-II implies $\frac{\Gamma_{H^+}}{m_{H^+}} \approx 3G_F m_t^2/4\sqrt{2}\pi\tan\beta^2$, which leads to $0.3 \lesssim \tan\beta \lesssim 130$. However, in the 2HDM-III we have that $\frac{\Gamma_{H^+}}{m_{H^+}} \approx (3G_F m_t^2/4\sqrt{2}\pi\tan\beta^2)\{1/[1 - (\tilde{\chi}^u_{33}/\sqrt{2}\cos\beta)]\}^2$, and we have checked numerically that this leads to $0.08 < \tan\beta < 200$ when $|\tilde{\chi}^u_{33}| \approx 1$ and $0.3 < \tan\beta < 130$ as long as $|\tilde{\chi}^u_{33}| \to 0$ recovering the result for the case of the 2HDM-II [7,38]. In this sense, if we consider the constraints imposed by the perturbativity bound, a portion of the low $\tan\beta$ appearing in some graphs would be excluded. However, we have decided to keep that range both to show the behavior of the quantities of interest and also because we have to keep in mind that such criteria (perturbativity) should be taken as an order of magnitude constraint.

The expressions for the charged Higgs boson decay widths $H^+ \to u_i\bar{d}_j$ are of the form

$$\Gamma(H^+ \to u_i\bar{d}_j) = \frac{3g^2}{32\pi M_W^2 m_{H^+}^3}\lambda^{1/2}(m_{H^+}^2, m_{u_i}^2, m_{d_j}^2) \times \left(\frac{1}{2}[m_{H^+}^2 - m_{u_i}^2 - m_{d_j}^2](S_{ij}^2 + P_{ij}^2) - m_{u_i}m_{d_j}(S_{ij}^2 - P_{ij}^2)\right), \quad (11)$$

where λ is the usual kinematic factor $\lambda(a, b, c) = (a - b - c)^2 - 4bc$. When we replace $\tilde{\chi}_{ud} \to 0$, the formulas of the decay widths become those of the 2HDM-II: see, e.g., Ref. [2]. Furthermore, the expressions for the charged Higgs boson decay widths of the bosonic modes remain the same as in the 2HDM-II. Then the results for the branching ratios (BRs) are shown in Figs. 2–8 and have the following characteristics.

Scenario A.—In Fig. 2(a), we present the BRs for the channels $H^+ \to t\bar{b}$, $c\bar{b}$, $t\bar{s}$, $\tau^+\nu_\tau$, W^+h^0, and W^+A^0 as a function of m_{H^+}, for $\tan\beta = 0.1$ and fixing $m_{h^0} = 120$ GeV, $m_{A^0} = 300$ GeV, and the mixing angle $\alpha = \pi/2$. When $m_{H^+} < 175$ GeV, we can see that the dominant decay of the charged Higgs boson is via the mode $c\bar{b}$, with $\mathrm{BR}(H_i^+ \to c\bar{b}) \approx 1$, which will have important consequences for charged Higgs boson production through $c\bar{b}$ fusion at the LHC and may serve as a distinctive feature of this model. For the case 175 GeV $< m_{H^+} <$ 180 GeV, the mode $t\bar{s}$ is relevant, which is also very different from the 2HDM-II and becomes an interesting phenomenological consequence of the 2HDM-III. We can also observe that, for $m_{H^+} >$ 180 GeV, the decay mode $t\bar{b}$ is dominant (as in the 2HDM-II). Now, from Fig. 2(b), where $\tan\beta = 1$, we

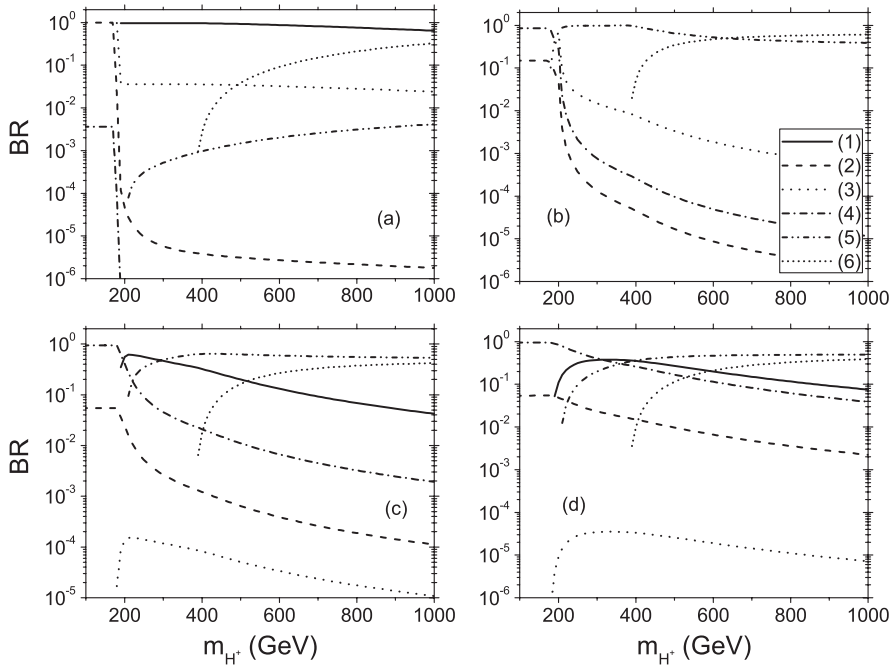

FIG. 2. The figure shows the BRs of the H^+ decaying into the principal modes in scenario A, taking $\tilde{\chi}^u_{ij} = 1$, $\tilde{\chi}^d_{ij} = 1$, $m_{h^0} = 120$ GeV, $m_{A^0} = 300$ GeV, and $\alpha = \pi/2$ for (a) $\tan\beta = 0.1$, (b) $\tan\beta = 1$, (c) $\tan\beta = 15$, and (d) $\tan\beta = 70$. The lines in each graph correspond to (1) $\mathrm{BR}(H^+ \to t\bar{b})$, (2) $\mathrm{BR}(H^+ \to c\bar{b})$, (3) $\mathrm{BR}(H^+ \to t\bar{s})$, (4) $\mathrm{BR}(H^+ \to \tau^+\nu_\tau)$, (5) $\mathrm{BR}(H^+ \to W^+h^0)$, and (6) $\mathrm{BR}(H^+ \to W^+A^0)$.

find that the dominant decay mode is into $\tau^+\nu_\tau$ for the range $m_{H^+} < 175$ GeV, and again for 175 GeV $< m_{H^+} <$ 180 GeV the mode $t\bar{s}$ is the leading one, but for 180 GeV $< m_{H^+} < 600$ GeV, the decay channel W^+h^0 becomes relevant, whereas for the range 600 GeV $< m_{H^+}$ the mode W^+A^0 is dominant. It is convenient to mention that this subscenario is special for the mode $t\bar{b}$, because its decay width is zero at the tree level, since the CKM contribution is canceled exactly with the terms of the four-zero texture implemented for the Yukawa coupling of the 2HDM-III. Then [see Fig. 2(c)] for the case with $\tan\beta = 15$, one gets that $\mathrm{BR}(H^+ \to \tau^+\nu_\tau) \approx 1$ when $m_{H^+} < 180$ GeV. However, for 180 GeV $< m_{H^+} <$ 300 GeV, the dominant decay of the charged Higgs boson is the mode $t\bar{b}$, while in the range 300 GeV $< m_{H^+}$, the decay channel W^+h^0 is also relevant. For $\tan\beta = 70$, we show in Fig. 2(d) that the dominant decay of the charged Higgs boson is the mode $\tau^+\nu_\tau$, when $m_{H^+} < 300$ GeV, but that, for 300 GeV $< m_{H^+} < 400$ GeV, the decay channel $t\bar{b}$ becomes the leading one, whereas for the range 400 GeV $< m_{H^+}$, the mode W^+h^0 is again dominant.

Scenario B.—In Fig. 3, we present the BRs of the channels $H^+ \to t\bar{b}$, $c\bar{b}$, $t\bar{s}$, $\tau^+\nu_\tau$, W^+h^0, and W^+A^0 as a function of m_{H^+}. From Fig. 3(a), we observe that for $\tan\beta = 0.1$, when $m_{H^+} < 175$ GeV, the dominant decay of the charged Higgs boson is the mode $c\bar{b}$, with $\mathrm{BR}(H^+_i \to c\bar{b}) \approx 1$. When 175 GeV $< m_{H^+} <$ 180 GeV, the mode $t\bar{s}$ is important, and for $m_{H^+} >$ 180 GeV the decay mode $t\bar{b}$ becomes the leading one. From Fig. 3(b), we see that, for $\tan\beta = 1$, the dominant decay mode is now into $\tau^+\nu_\tau$ for $m_{H^+} < 175$ GeV, while in the range 175 GeV $< m_{H^+} <$ 180 GeV the mode $t\bar{s}$ is relevant. For 180 GeV $< m_{H^+} <$ 500 GeV the decay channel $t\bar{b}$ becomes the leading one, whereas for the range 500 GeV $< m_{H^+}$ the mode W^+A^0 is dominant. From Fig. 3(c), with $\tan\beta = 15$, one gets that $\mathrm{BR}(H^+_i \to \tau^+\nu_\tau) \approx 1$ for $m_{H^+} <$ 180 GeV. For 180 GeV $< m_{H^+}$, the dominant decay of the charged Higgs boson is instead the mode W^+h^0. Then, for $\tan\beta = 70$, we show in Fig. 3(d) that the dominant decay of the charged Higgs state is via the mode $\tau^+\nu_\tau$ when $m_{H^+} < 350$ GeV, while for 350 GeV $< m_{H^+}$ the decay channel W^+h^0 becomes the leading one.

Scenario C.—In Fig. 4, we show the corresponding plots for the BRs of the channels $H^+ \to t\bar{b}$, $c\bar{b}$, $t\bar{s}$, $\tau^+\nu_\tau$, W^+h^0, and W^+A^0 as a function of m_{H^+}. For $\tan\beta = 0.1$, as one can see in Fig. 4(a), the mode $c\bar{b}$ is dominant when $m_{H^+} <$ 170 GeV, but for 175 GeV $< m_{H^+} <$ 180 GeV the mode $t\bar{s}$ is relevant, while for 180 GeV $< m_{H^+}$ the mode $t\bar{b}$ becomes dominant. For $\tan\beta = 1$, we observe from Fig. 4(b) that the dominant decay modes are $\tau^+\nu_\tau$ in the range $m_{H^+} <$ 170 GeV, $t\bar{s}$ for 175 GeV $< m_{H^+} <$ 180 GeV, W^+h^0 for 180 GeV $< m_{H^+} <$ 600 GeV, and W^+A^0 when 600 GeV $< m_{H^+}$. For $\tan\beta = 15$, as shown in Fig. 4(c), the relevant decay channels are $\tau^+\nu_\tau$ in the range $m_{H^+} < 180$ GeV, $t\bar{b}$ when 180 GeV $< m_{H^+} <$ 300 GeV, and W^+h^0 for 300 GeV $< m_{H^+}$. In Fig. 4(d), for $\tan\beta = 70$, we observe that $\tau^+\nu_\tau$ dominates when $m_{H^+} < 180$ GeV, but when 180 GeV $< m_{H^+} <$ 900 GeV the mode $t\bar{b}$ is the leading

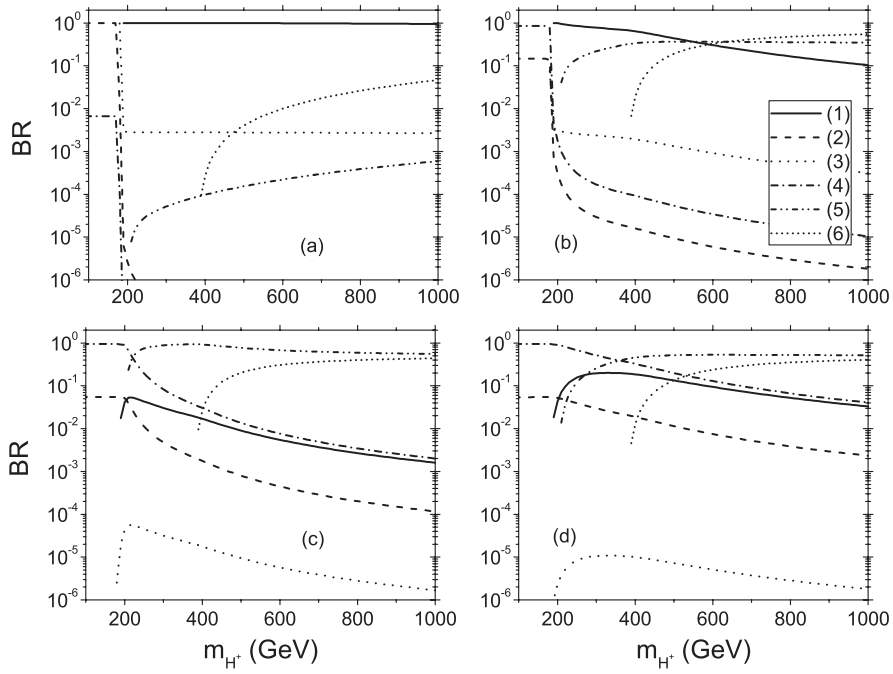

FIG. 3. The same as in Fig. 2 but taking $\tilde{\chi}^u_{ij} = 0.1$, $\tilde{\chi}^d_{ij} = 1$ (scenario B).

one, whereas for 900 GeV $< m_{H^+}$ the mode W^+h^0 is the most relevant one.

Scenario D.—In Fig. 5, we present plots for the BRs of the channels $t\bar{b}$, $c\bar{b}$, $t\bar{s}$, $\tau^+\nu_\tau$, W^+h^0, and W^+A^0 as a function of m_{H^+}. For $\tan\beta = 0.1$, we show in Fig. 5(a) that the dominant decay modes for the H^+ are $c\bar{b}$ in the range $m_{H^+} < 175$ GeV, $t\bar{s}$ when 175 GeV $< m_{H^+} <$ 180 GeV, and $t\bar{b}$ for 180 GeV $< m_{H^+}$. For $\tan\beta = 1$, we show in Fig. 5(b) that the mode $\tau^+\nu_\tau$ is dominant in the range $m_{H^+} < 175$ GeV, whereas for 175 GeV $< m_{H^+} <$ 180 GeV the relevant decay channel is $t\bar{s}$, while the mode $t\bar{b}$ dominates for 180 GeV $< m_{H^+} <$ 550 GeV and the mode W^+A^0 does so when 550 GeV $< m_{H^+}$. For $\tan\beta = 15$, we observe in Fig. 5(c) that the relevant decay

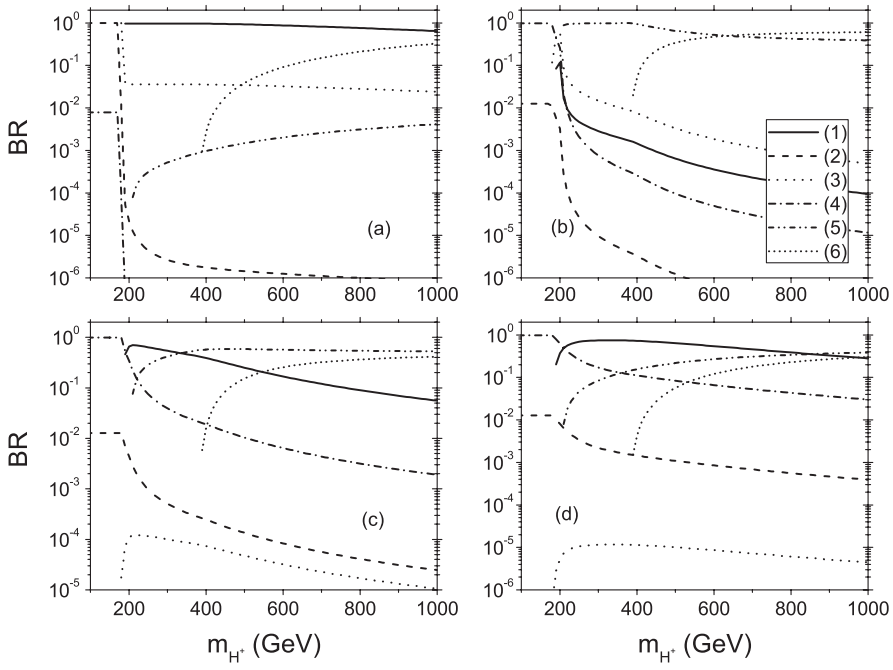

FIG. 4. The same as in Fig. 2, but taking $\tilde{\chi}^u_{ij} = 1$, $\tilde{\chi}^d_{ij} = 0.1$ (scenario C).

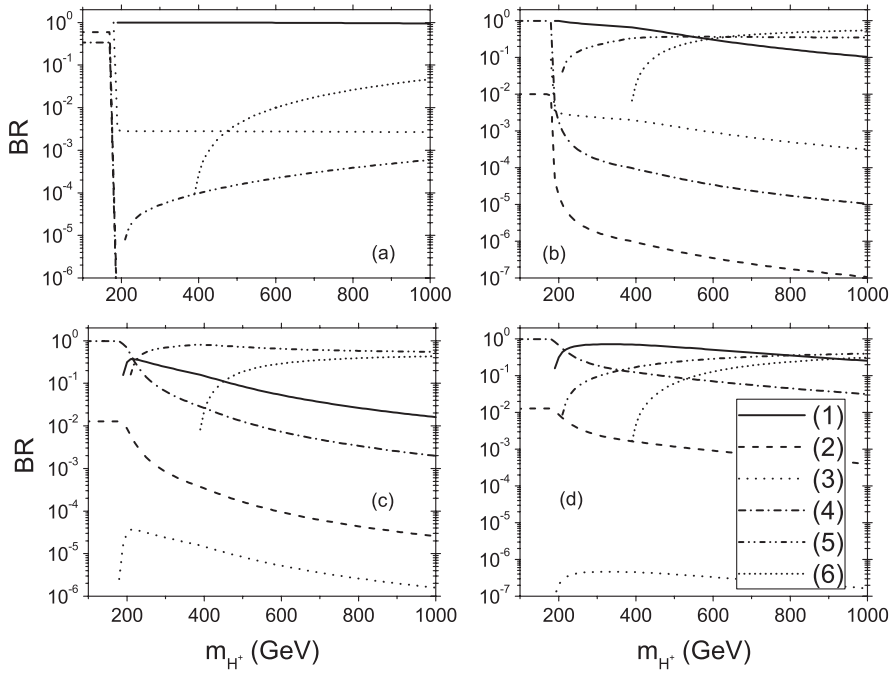

FIG. 5. The same as in Fig. 2, but taking $\tilde{\chi}^{u}_{ij} = 0.1$, $\tilde{\chi}^{d}_{ij} = 0.1$ (scenario D).

channels are $\tau^+\nu_\tau$ in the range $m_{H^+} < 250$ GeV and W^+h^0 for 250 GeV $< m_{H^+}$. Finally, for $\tan\beta = 70$ [see Fig. 5(d)], we obtain that, when $m_{H^+} < 230$ GeV, the mode $\tau^+\nu_\tau$ becomes the most important one but, for 230 GeV $< m_{H^+} <$ 800 GeV, the channel $t\bar{b}$ is the leading one, whereas, for 800 GeV $< m_{H^+}$, the mode W^+h^0 is the dominant one.

In order to cover further the Higgs sector in our analysis, it is appropriate to also mention how the previous results change with m_{h^0}, m_{A^0}, and α. Regarding the former two, clearly, the later the neutral Higgs boson mass, the later the corresponding $H^\pm$ decay channel will onset. Regarding the latter, we adopted two further choices $\alpha = \beta$ and 0 in all scenarios previously studied. In general, the behavior of

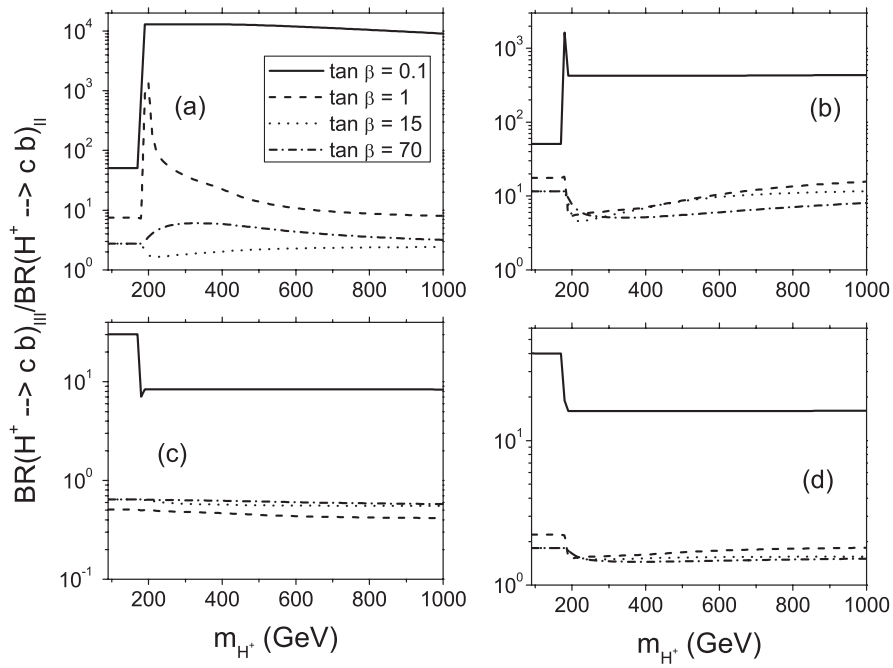

FIG. 6. The figure shows the $\mathrm{BR}(H^+ \to c\bar{b})_{\mathrm{III}}/\mathrm{BR}(H^+ \to c\bar{b})_{\mathrm{II}}$ vs m_{H^+}, taking $\tan\beta = 0.1$, 1, 15, and 70 for (a) $\tilde{\chi}^{u,d}_{ij} = 1$, (b) $\tilde{\chi}^{u,d}_{ij} = -1$, (c) $\tilde{\chi}^{u,d}_{ij} = 0.1$, and (d) $\tilde{\chi}^{u,d}_{ij} = -0.1$.

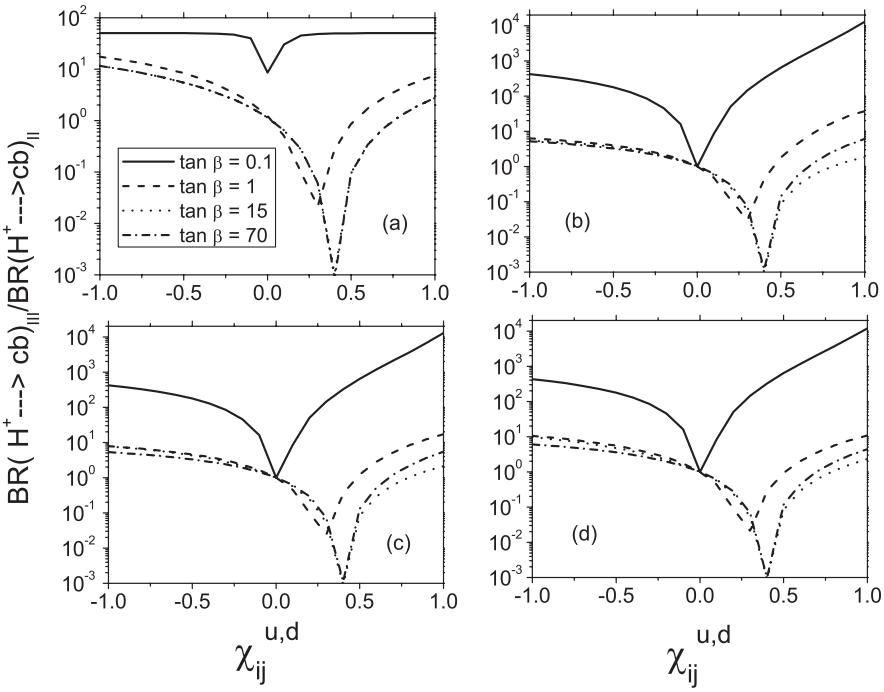

FIG. 7. The figure shows the $\mathrm{BR}(H^+ \to c\bar{b})_{\mathrm{III}}/\mathrm{BR}(H^+ \to c\bar{b})_{\mathrm{II}}$ vs $\tilde{\chi}^{u,d}_{ij}$, taking $\tan\beta = 0.1$, 1, 15, and 70 for (a) $m_{H^+} = 150$ GeV, (b) $m_{H^+} = 300$ GeV, (c) $m_{H^+} = 450$ GeV, and (d) $m_{H^+} = 600$ GeV.

the decay modes of the charged Higgs boson is similar to the cases presented above, except for the decay channel Wh^0. For $\alpha = 0$, this mode has $\mathrm{BR} < 10^{-3}$ when $\tan\beta$ is large. However, for $\tan\beta < 1$, it becomes the dominant one. In the case $\alpha = \beta$, the decay channel Wh^0 can be dominant with a BR that could be $O(1)$.

As a general lesson from this section and distinctive features of our 2HDM-III, we can see that both decay modes W^+h^0 and $c\bar{b}$ become very relevant phenomenologically, effectively of $O(1)$ for some of the scenarios considered. Therefore, we want to study next the general behavior of these decay modes, in relation to the 2HDM-II

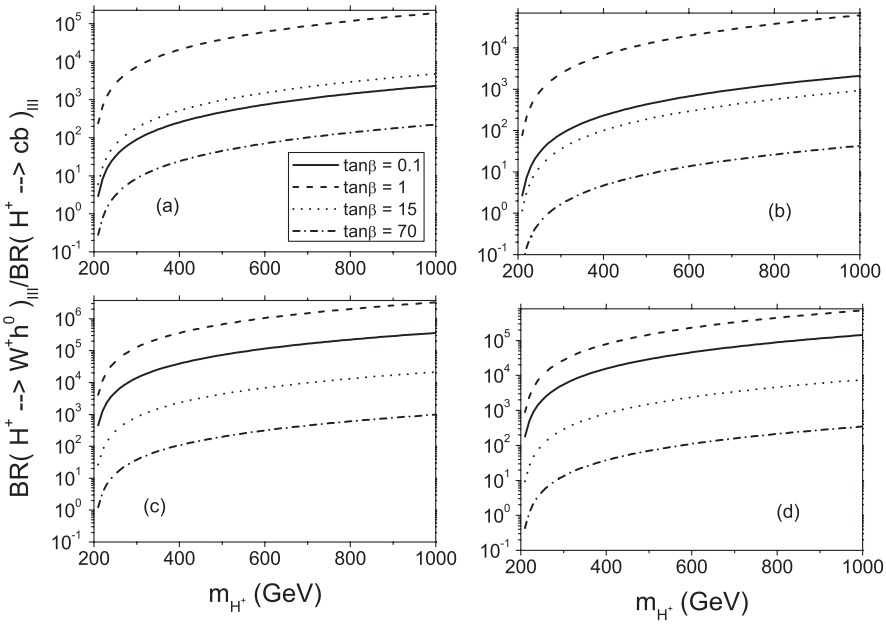

FIG. 8. The figure shows the $\mathrm{BR}(H^+ \to W^+h^0)_{\mathrm{III}}/\mathrm{BR}(H^+ \to c\bar{b})_{\mathrm{III}}$ vs m_{H^+}, taking $\tan\beta = 0.1$, 1, 15, and 70 for (a) $\tilde{\chi}^{u,d}_{ij} = 0.1$, (b) $\tilde{\chi}^{u,d}_{ij} = -0.1$, (c) $\tilde{\chi}^{u,d}_{ij} = 1$, and (d) $\tilde{\chi}^{u,d}_{ij} = -1$.

case. In order to compare the 2HDM-III results with those in the 2HDM-II, we show in Fig. 6 the ratio $\mathrm{BR}(H^+ \to c\bar{b})_{\mathrm{III}}/\mathrm{BR}(H^+ \to c\bar{b})_{\mathrm{II}}$ vs m_{H^+}, taking again $\tan\beta = 0.1$, 1, 15, and 70, for (a) $\tilde{\chi}^{u,d}_{ij} = 1$, (b) $\tilde{\chi}^{u,d}_{ij} = -1$, (c) $\tilde{\chi}^{u,d}_{ij} = 0.1$, and (d) $\tilde{\chi}^{u,d}_{ij} = -0.1$. We observe that the mode $c\bar{b}$ is important when $200\ \mathrm{GeV} < m_{H^+} < 300\ \mathrm{GeV}$ and for $0.1 \leq \tan\beta \leq 1$, taking $\tilde{\chi}^{u,d}_{ij} = 1$. Now, in Fig. 7, we present the behavior of the ratio $\mathrm{BR}(H^+ \to c\bar{b})_{\mathrm{III}}/\mathrm{BR}(H^+ \to c\bar{b})_{\mathrm{II}}$ as a function of $\chi^{u,d}_{i,j}$, for the cases (a) $m_{H^+} = 150\ \mathrm{GeV}$, (b) $m_{H^+} = 300\ \mathrm{GeV}$, (c) $m_{H^+} = 450\ \mathrm{GeV}$, and (d) $m_{H^+} = 600\ \mathrm{GeV}$. Again, one can see that the largest enhancement arises when $m_{H^+} = 300\ \mathrm{GeV}$ and $\tilde{\chi}^{u,d}_{ij} = 1$. Finally, specific to the 2HDM-III, we show in Fig. 8 the ratio $\mathrm{BR}(H^+ \to W^+h^0)_{\mathrm{III}}/\mathrm{BR}(H^+ \to c\bar{b})_{\mathrm{III}}$ vs m_{H^+}, taking $\tan\beta = 0.1$, 1, 15, and 70, for (a) $\tilde{\chi}^{u,d}_{ij} = 0.1$, (b) $\tilde{\chi}^{u,d}_{ij} = -0.1$, (c) $\tilde{\chi}^{u,d}_{ij} = 1$, and (d) $\tilde{\chi}^{u,d}_{ij} = 1$. We find that $\mathrm{BR}(H^+ \to W^+h^0)_{\mathrm{III}}$ is much larger than $\mathrm{BR}(H^+ \to c\bar{b})_{\mathrm{III}}$ when $\tilde{\chi}^{u,d}_{ij} = 1$ and the mass of the charged Higgs boson is close to the upper limit obtained by unitarity conditions, which is about 800 GeV [26]. Thus, we find that the effect of the modified Higgs couplings typical of the 2HDM-III shows up clearly in the pattern of charged Higgs boson decays, which can be very different from the 2HDM-II case and thus enrich the possibilities to search for $H^\pm$ states at current (Tevatron) and future (LHC, ILC/CLIC) machines.

IV. CHARGED HIGGS BOSON PRODUCTION AT THE LHC

The production of charged Higgs bosons at hadron colliders has been evaluated in early [21] (also for the Superconducting Super Collider) and more recent [22] (for the LHC) literature, mainly for the 2HDM-II and its SUSY realization (i.e., the MSSM). In these two scenarios, when kinematically allowed, the top quark decay channel $t \to bH^+$ is the dominant $H^\pm$ production mechanism. Instead, above the threshold for such a decay, the dominant $H^\pm$ production reaction is gluon-gluon fusion into a 3-body final state, i.e., $gg \to tbH^\pm$.[4] Both processes depend on the coupling $H^- t\bar{b}$ and are therefore sensitive to the modifications that arise in the 2HDM-III for this vertex. However, detection of the final state will depend on the charged Higgs boson decay mode, which could include a complicated final state, that could in turn be difficult to reconstruct. For these reasons, it is very important to look for other production channels, which may be easier to reconstruct. In this regard, the s-channel production of charged Higgs bosons, through the mechanism of $c\bar{b}$ fusion, could help to make more viable the detection of several charged Higgs boson decay channels [27].

[4]In fact, these two mechanisms are intimately related; see below.

Here we shall evaluate the predictions of the 2HDM-III for the $t \to bH^+$ (and sH^+) decay rate plus the $c\bar{b}$- as well as the gg-fusion mechanisms (hereafter, referred to as "direct" and "indirect" $H^\pm$ production, respectively).

A. The decays $t \to H^+b$, H^+s

We shall discuss here the charged Higgs boson interactions with heavy quarks (t, b, c, s) and their implications for charged Higgs boson production through top quark decays. In order to study the top quark BRs, besides the SM decay mode $t \to bW^+$, we need to consider both decays $t \to bH^+$ and $t \to sH^+$, because these modes could both be important for several parameter configurations within our model. The decay width of these modes takes the following form:

$$\Gamma(t \to d_j H^+) = \frac{g^2}{128\pi m_W^2 m_t^3}\lambda^{1/2}(m_t^2, m_{H^+}^2, m_b^2)([(m_t + m_b)^2 - m_{H^+}^2]S_{3j}^2 + [(m_t + m_b)^2 - m_{H^+}^2]P_{3j}^2), \quad (12)$$

where λ is the usual kinematic factor $\lambda(a, b, c) = (a - b - c)^2 - 4bc$, $j = 2$ for the mode sH^+, and $j = 3$ for the mode bH^+. Furthermore, we shall neglect the decay width for the light fermion generations. If one takes $\tilde{\chi}_{i,j} \to 0$, the formulas for the decay width reduce to the 2HDM-II case: see, e.g., [2].

We have explored several theoretically allowed regions within our scenario, which are constrained by using the bounds on the $\mathrm{BR}(t \to bH^+)$. In the so-called "tauonic Higgs model" [23], the decay mode $(H^+ \to \tau^+\nu_\tau)$ dominates the charged Higgs boson decay width, and $\mathrm{BR}(t \to bH^+)$ is constrained to be less than 0.4 at 95% C.L. [23]. However, if no assumption is made on the charged Higgs boson decay, $\mathrm{BR}(t \to bH^+)$ is constrained to be less than 0.91 at 95% C.L. [23]. However, the combined LEP data exclude a charged Higgs boson with mass less than 79.3 GeV at 95% C.L., a limit valid for an arbitrary $\mathrm{BR}(H^+ \to \tau^+\nu_\tau)$ [25]. Thus, in order to perform our analysis, we need to discuss all of the charged Higgs boson decays following the steps of our previous paper [19]. In the present section, we take all charged Higgs boson decays relevant for masses below that of the top quark, thus including the modes $\tau^+\nu_\tau$, $t\bar{s}$, $c\bar{b}$, W^+h^0, and W^+A^0. As usual, we refer to our four benchmark scenarios.

Scenario A.—Remember that this scenario was defined by taking $\tilde{\chi}^u_{ij} = 1$ and $\tilde{\chi}^d_{ij} = 1$, while for $\tan\beta$ we considered the values $\tan\beta = 0.1$, 1, 15, and 70. In Fig. 9, we present plots of $\mathrm{BR}(t \to bH^+)$ vs m_H^+ and $\mathrm{BR}(t \to sH^+)$ vs m_{H^+}. We can observe that a charged Higgs boson within the mass range $80\ \mathrm{GeV} < m_{H^+} < 170\ \mathrm{GeV}$ and for $1 < \tan\beta < 70$ satisfies the constraint $\mathrm{BR}(t \to bH^+) < 0.4$. Furthermore, from the plots of Fig. 2, we can see that in this scenario the dominant decay mode is into $\tau^+\nu_\tau$ for $\tan\beta = 1$, 15, and 70; therefore, we fall within the scope of the tauonic Higgs model, so that $\mathrm{BR}(t \to H^+b) \leq 0.4$

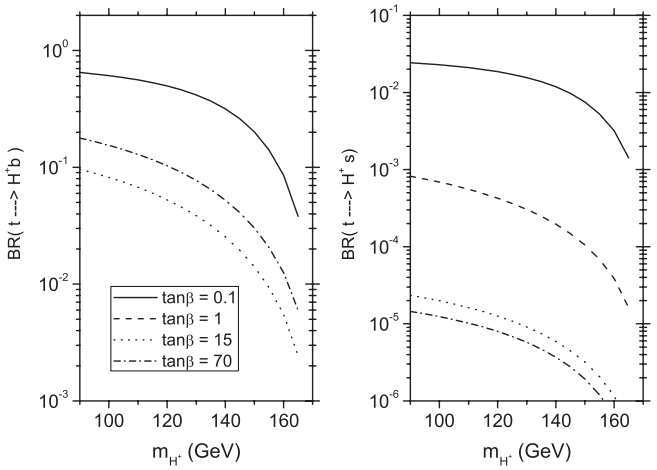

FIG. 9. It is plotted: the BR($t \to bH^+$) vs m_{H^+} (left); the BR($t \to sH^+$) vs m_{H^+} (right). Here is for scenario A, obtained by taking $\tilde{\chi}^u_{ij} = 1$ and $\tilde{\chi}^d_{ij} = 1$, for tan$\beta = 0.1$ (solid line), 1 (dashed line), 15 (dotted line), and 70 (dashed-dotted line).

applies. However, for the case tan$\beta = 0.1$, the dominant decay of the charged Higgs boson is the mode $c\bar{b}$, and the mode $t \to bH^+$ satisfies the constraint BR($t \to bH^+$) $<$ 0.9 in the range described above.

Scenario B.—In Fig. 10, we present similar plots for the case $\tilde{\chi}^u_{ij} = 0.1$ and $\tilde{\chi}^d_{ij} = 1$, taking tan$\beta = 0.1$, 1, 15, and 70. We can observe that the mode $t \to bH^+$ satisfies the constraint BR($t \to bH^+$) < 0.4 within the ranges 80 GeV $< m_{H^+} <$ 170 GeV and $1 <$ tan$\beta < 70$. Thus, from Fig. 3, we can see that in this range the dominant decay mode is into $\tau^+\nu_\tau$; therefore, this setups also falls within the realm of the tauonic Higgs model, so that BR($t \to H^+b$) ≤ 0.4 must hold in this scenario. For tan$\beta = 0.1$, the dominant decay of the charged Higgs boson is $c\bar{b}$, and thus the channel $t \to bH^+$ must satisfy the constraint BR($t \to bH^+$) < 0.9, which is fulfilled in the range studied.

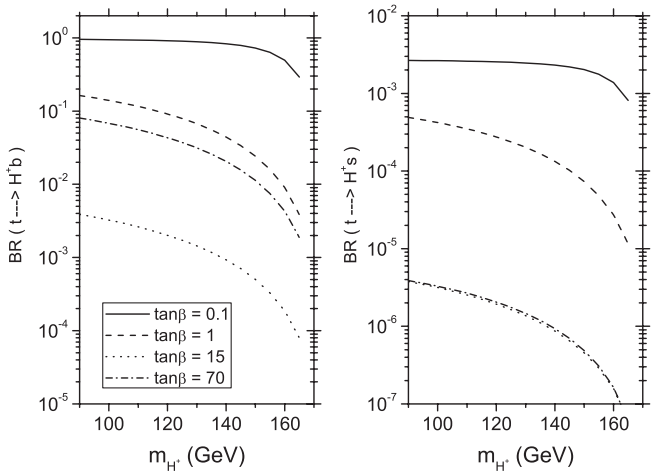

FIG. 10. The same as in Fig. 9 but taking $\tilde{\chi}^u_{ij} = 0.1$ and $\tilde{\chi}^d_{ij} = 1$ (scenario B).

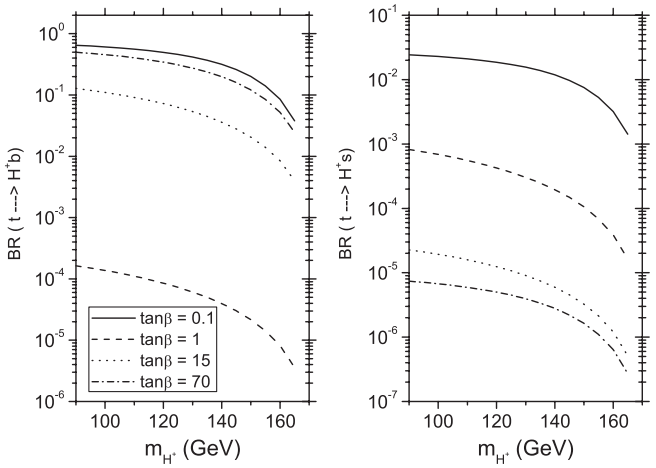

FIG. 11. The same as in Fig. 9 but taking $\tilde{\chi}^u_{ij} = 1$ and $\tilde{\chi}^d_{ij} = 0.1$ (scenario C).

Scenario C.—In Fig. 11, we present the corresponding plots for the case $\tilde{\chi}^u_{ij} = 1$ and $\tilde{\chi}^d_{ij} = 0.1$, taking again tan$\beta = 0.1$, 1, 15, and 70. We can observe that the mode $t \to bH^+$ satisfies the constraint BR($t \to bH^+$) < 0.4 in the range 80 GeV $< m_{H^+} <$ 170 GeV and $1 <$ tan$\beta < 70$. Similarly, as in scenario A, for tan$\beta = 0.1$ the dominant decay of the charged Higgs boson is the mode $c\bar{b}$, and thus the mode $t \to bH^+$ must satisfy the constraint BR($t \to bH^+$) < 0.9, indeed satisfied in the range analyzed here.

Scenario D.—Recall that this was defined by taking $\tilde{\chi}^u_{ij} = 0.1$ and $\tilde{\chi}^d_{ij} = 0.1$. In Fig. 12, we present the usual plots of the BR($t \to bH^+$) and BR($t \to bH^+$) vs m_{H^+}. One can see that, for charged Higgs boson masses within the range 80 GeV $< m_{H^+} <$ 170 GeV and $1 <$ tan$\beta < 70$, the model fulfills the constraint BR($t \to bH^+$) < 0.4. Furthermore, for tan$\beta = 0.1$, the dominant decay of the charged Higgs boson is the mode $c\bar{b}$, and thus the mode

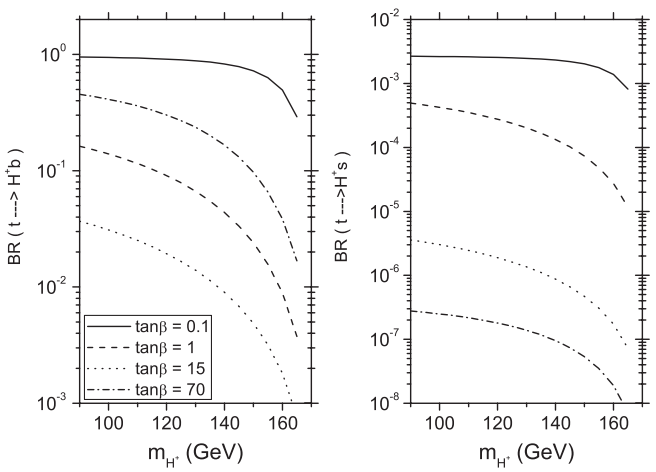

FIG. 12. The same as in Fig. 9 but taking $\tilde{\chi}^u_{ij} = 0.1$ and $\tilde{\chi}^d_{ij} = 0.1$ (scenario D).

$t \to bH^+$ satisfies the constraint $\mathrm{BR}(t \to bH^+) < 0.9$ in the range studied.

In short, as the bottom line of these exercises, we have identified regions of the 2HDM-III parameter space where a charged Higgs mass below $m_t - m_b$ has not been excluded by the Tevatron. Therefore, the LHC is best positioned in order to probe charged Higgs bosons with such masses.

B. Direct production of charged Higgs bosons at the LHC

The $H^\pm \bar{q} q'$ vertex with large flavor mixing coupling, that arises in the 2HDM-III, enables the possibility of studying the production of charged Higgs boson via the s-channel production mechanism $c\bar{b} \to H^+ + \text{c.c.}$ This process was discussed first by Ref. [27], both within top color models and a simplified version of the 2HDM-III. Then the SUSY case was discussed in [39,40]. Here we perform a detailed study of this mechanism within the 2HDM-III, paying special attention to the effects induced by the assumed Yukawa texture on the charged Higgs boson couplings. Defining the $H^\pm \bar{q} q'$ coupling here as $C_L \frac{1-\gamma_5}{2} + C_R \frac{1+\gamma_5}{2}$, we can express the total cross section for H^+ direct production at hadron colliders as [27]

$$\sigma(h_1 h_2 (c\bar{b}) \to H^+ X) = \frac{\pi}{12 s} (|C_L|^2 + |C_R|^2) I^{h_1,h_2}_{c,\bar{b}}, \quad (13)$$

where

$$I^{h_1,h_2}_{c,\bar{b}} = \int_\tau^1 \frac{dx}{x} [f^{h_1}_c(x, \tilde{Q}^2) f^{h_2}_{\bar{b}}(\tau/x, \tilde{Q}^2) + f^{h_1}_{\bar{b}}(x, \tilde{Q}^2) f^{h_2}_c(\tau/x, \tilde{Q}^2)] \quad (14)$$

and $\tau = m^2_{H^\pm}/s$. The parton distribution functions $f^{h_i}_q(x, \tilde{Q}^2)$ used here are from [41], with scale choice $\tilde{Q}^2 = m^2_{H^+}$.

From Eq. (6) we see that, for the case of the 2HDM-III, C_L and C_R entering the subprocess $c\bar{b} \to H^+$ are given by

$$C_L \equiv C^{\mathrm{III}}_L = -\frac{ig}{\sqrt{2} M_W} \sum_{l=1}^{3} \left[\cot\beta m_c \delta_{2l} - \frac{\csc\beta}{\sqrt{2}} \sqrt{m_c m_{u_l}} \tilde{\chi}^u_{2l} \right] (V_{\mathrm{CKM}})_{l3} \quad (15)$$

and

$$C_R \equiv C^{\mathrm{III}}_R = -\frac{ig}{\sqrt{2} M_W} \sum_{l=1}^{3} \left[\tan\beta m_{d_l} \delta_{l3} - \frac{\sec\beta}{\sqrt{2}} \sqrt{m_{d_l} m_{d_3}} \tilde{\chi}^d_{l3} \right] \times (V_{\mathrm{CKM}})_{2l}. \quad (16)$$

We notice here that Eqs. (15) and (16) reduce to the case of the 2HDM-II if one takes

$$C_L \equiv C^{\mathrm{II}}_L = -\frac{ig}{\sqrt{2} M_W} \cot\beta m_c (V_{\mathrm{CKM}})_{23} \quad (17)$$

and

$$C_R \equiv C^{\mathrm{II}}_R = -\frac{ig}{\sqrt{2} M_W} \tan\beta m_b (V_{\mathrm{CKM}})_{23}. \quad (18)$$

In Fig. 13, we present plots for the total cross section rates of process $h_1 h_2 (c\bar{b}) \to H^+ X$ as a function of m_{H^+} in the framework of the 2HDM-III, by taking $\tilde{\chi}^d_{l3} = 1$ and $\tilde{\chi}^u_{2l} = 1$ ($l = 1, 2, 3$), at LHC energies ($\sqrt{s} = 14$ TeV), for the cases (a) $\tan\beta = 0.1$, (b) $\tan\beta = 1$, (c) $\tan\beta = 15$, and (d) $\tan\beta = 70$. The sum over l is performed over all three quark families, and we take for the quark masses $m_u = 2.55$ MeV, $m_d = 5.04$ MeV, $m_c = 1.27$ GeV, $m_s = 104$ MeV, $m_b = 4.20$ GeV, and $m_t = 171.2$ GeV [25]. We have checked numerically that the term proportional to $\frac{1}{2}\csc^2\beta m_c m_t |\tilde{\chi}^u_{23} (V_{\mathrm{CKM}})_{33}|^2$ provides the most important contribution to the cross section rates and dominates by far for $\tilde{\chi}^u_{23} \approx 1$. On the other hand, the expected integrated luminosity at the LHC is of the order 10^5 pb^{-1}, and, given that $\sigma \gtrsim 10^{-5}$ pb even for $\tan\beta = 70$ and $m_{H^+} \lesssim 600$ GeV, we can conclude that, in the context of the 2HDM-III, it is likely that a charged Higgs boson could be observed at LHC energies by exploiting direct production.

In Fig. 14, we present results for the total cross section rates of process $h_1 h_2 (c\bar{b}) \to H^+ X$ as a function of m_{H^+} in the 2HDM-II at LHC energies ($\sqrt{s} = 14$ TeV), by taking $(V_{\mathrm{CKM}})_{23} = 4.16 \times 10^{-2}$ and $(V_{\mathrm{CKM}})_{33} \approx 1$, for the cases (a) $\tan\beta = 0.1$, (b) $\tan\beta = 1$, (c) $\tan\beta = 15$, and (d) $\tan\beta = 70$. As we have already said, the expected integrated luminosity at the LHC is of the order

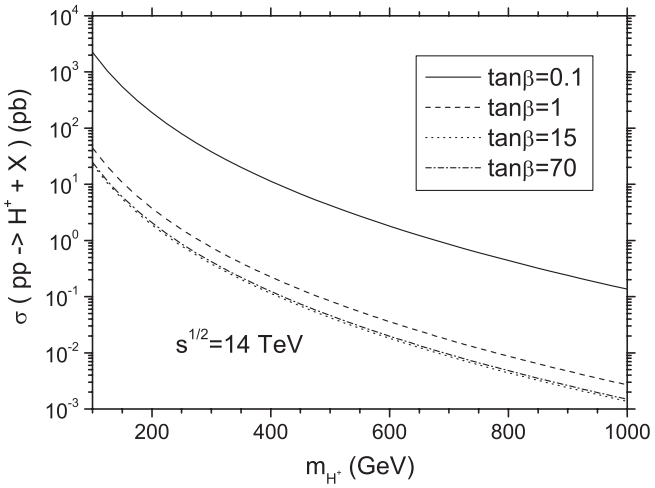

FIG. 13. The figure shows the total cross section rates of process $h_1 h_2 (c\bar{b}) \to H^+ X$ as a function of m_{H^+} in the 2HDM-III at LHC energies ($\sqrt{s} = 14$ TeV), by taking $\tilde{\chi}^d_{l3} = 1$ and $\tilde{\chi}^u_{2l} = 1$ ($l = 1, 2, 3$). The lines correspond to $\tan\beta = 0.1$, $\tan\beta = 1$, $\tan\beta = 15$, and $\tan\beta = 70$.

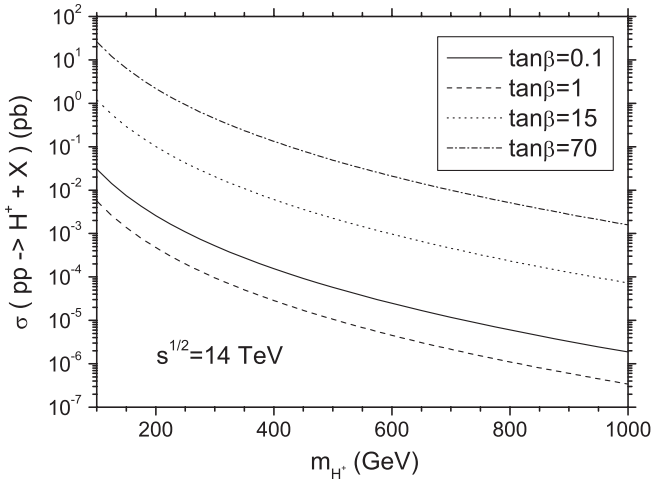

FIG. 14. The figure shows the total cross section rates of process $h_1h_2(c\bar{b}) \to H^+X$ as a function of m_{H^+} in the 2HDM-II at LHC energies ($\sqrt{s} = 14$ TeV), by taking $(V_{\rm CKM})_{23} = 4.16 \times 10^{-2}$ and $(V_{\rm CKM})_{33} \approx 1$. The lines correspond to $\tan\beta = 0.1$, $\tan\beta = 1$, $\tan\beta = 15$, and $\tan\beta = 70$.

10^5 pb^{-1}, and hence we also conclude from this figure that in the framework of the 2HDM-II we obtain production rates for the charged Higgs boson via $c\bar{b}$ fusion that may be detectable at LHC energies.

C. Indirect production of charged Higgs bosons at the LHC

We have found that, in some of the 2HDM-III scenarios envisaged here, light charged Higgs bosons could exist that have not been excluded by current experimental bounds, chiefly from LEP2 and Tevatron. Their discovery potential should therefore be studied in view of the upcoming LHC, and we shall then turn our attention now to presenting the corresponding hadroproduction cross sections via an indirect channel, i.e., other than as secondary products in (anti) top quark decays and via $c\bar{b}$ fusion, considered previously.

As dealt with so far, if the charged Higgs boson mass $m_{H^\pm}$ satisfies $m_{H^\pm} < m_t - m_b$, where m_t is the top quark mass and m_b the bottom quark mass, $H^\pm$ particles could be produced in the decay of on-shell (i.e., $\Gamma_t \to 0$) top (anti) quarks $t \to bH^+$ and the c.c. process, the latter being in turn produced in pairs via $q\bar{q}$ annihilation and gg fusion. We denote such a $H^\pm$ production channel as $q\bar{q}, gg \to t\bar{t} \to t\bar{b}H^- + \text{c.c.}$ [i.e., if due to (anti)top decays], while we use the notation $q\bar{q}, gg \to t\bar{b}H^- + \text{c.c.}$ to signify when further production diagrams are included.[5] In fact, owing to the large top decay width ($\Gamma_t \geq 1.5$ GeV) and due to the additional diagrams which do not proceed via direct $t\bar{t}$ production but yield the same final state $t\bar{b}H^- + \text{c.c.}$ [43–45], charged Higgs bosons could also be produced at and beyond the kinematic top decay threshold. The importance of these effects in the so-called "threshold" or "transition" region ($m_{H^\pm} \approx m_t$) was emphasized in various Les Houches proceedings [46,47] as well as in Refs. [42,48–50], so that the calculations of Refs. [43,44] (based on the appropriate $q\bar{q}, gg \to tbH^\pm$ description) are now implemented in HERWIG [51–54] and PYTHIA [55,56]. A comparison between the two generators was carried out in Ref. [48]. For any realistic simulation of $H^\pm$ production with $m_{H^\pm} \gtrsim m_t$, as can well be the case here, the use of either of these two implementations is of paramount importance.

Here, we use HERWIG version 6.510 in default configuration, by onsetting the subprocess *IPROC* = 3839, wherein we have overwritten the default MSSM/2HDM couplings and masses with those pertaining to the 2HDM-III: see Eqs. (7) and (8). The production cross sections are found in Figs. 15–18 for our usual scenarios: A ($\tilde{\chi}^u_{ij} = 1$ and $\tilde{\chi}^d_{ij} = 1$), B ($\tilde{\chi}^u_{ij} = 1$ and $\tilde{\chi}^d_{ij} = 0.1$), C ($\tilde{\chi}^u_{ij} = 0.1$ and $\tilde{\chi}^d_{ij} = 1$), and D ($\tilde{\chi}^u_{ij} = 0.1$ and $\tilde{\chi}^d_{ij} = 0.1$) As usual, we adopt our four choices of $\tan\beta$.

Altogether, by comparing the $q\bar{q}, gg \to t\bar{b}H^-_i + \text{c.c.}$ cross sections herein with, e.g., those of the MSSM in [6] or the 2HDM in [49,57], it is clear that the 2HDM-III rates can be very large, and thus the discovery potential in ATLAS and CMS can be substantial, particularly for a very light $H^\pm$, which may pertain to our 2HDM-III but not the MSSM or 2HDM-II. However, it is only by combining the production rates of this section with the decay ones of the previous ones that actual event numbers at the LHC can be predicted.

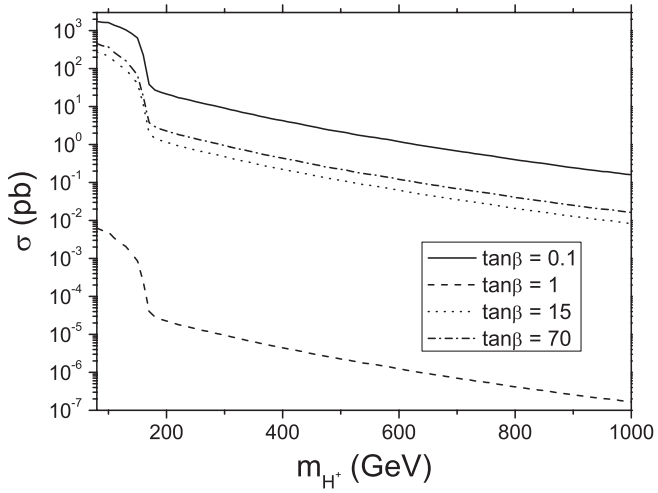

FIG. 15. The figure shows the cross sections of H^+ production at the LHC through the channel $q\bar{q}, gg \to t\bar{b}H^- + \text{c.c.}$ in scenario A ($\tilde{\chi}^u_{ij} = 1$ and $\tilde{\chi}^d_{ij} = 1$) and for $\tan\beta = 0.1$, 1, 15, and 70.

[5] Altogether, they represent the full gauge invariant set of Feynman graphs pertaining to the $2 \to 3$-body process with a $t\bar{b}H^-_i + \text{c.c.}$ final state: two for the case of $q\bar{q}$ annihilation and eight for gluon-gluon fusion; see, e.g., Eq. (1.1) of [42].

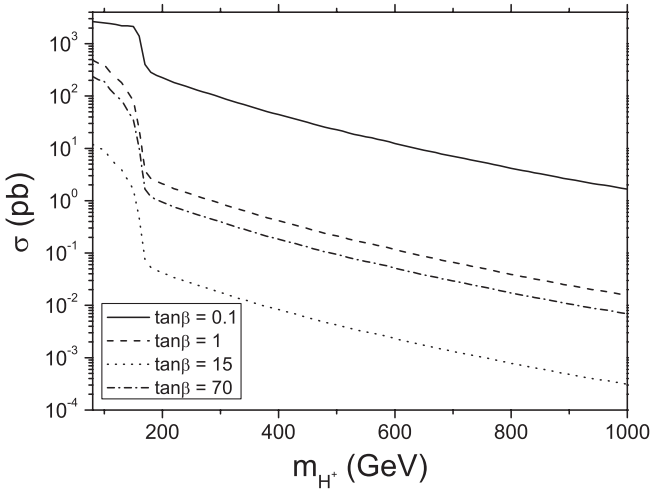

FIG. 16. The same as in Fig. 15 but taking $\tilde{\chi}^u_{ij} = 1$ and $\tilde{\chi}^d_{ij} = 0.1$ (scenario B).

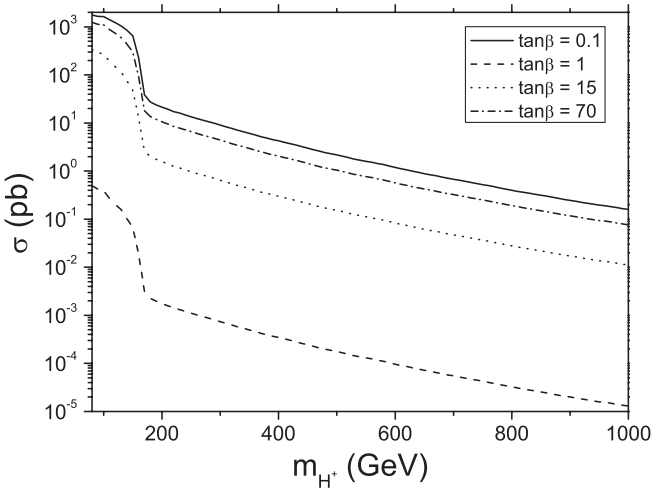

FIG. 17. The same as in Fig. 15 but taking $\tilde{\chi}^u_{ij} = 0.1$ and $\tilde{\chi}^d_{ij} = 1$ (scenario C).

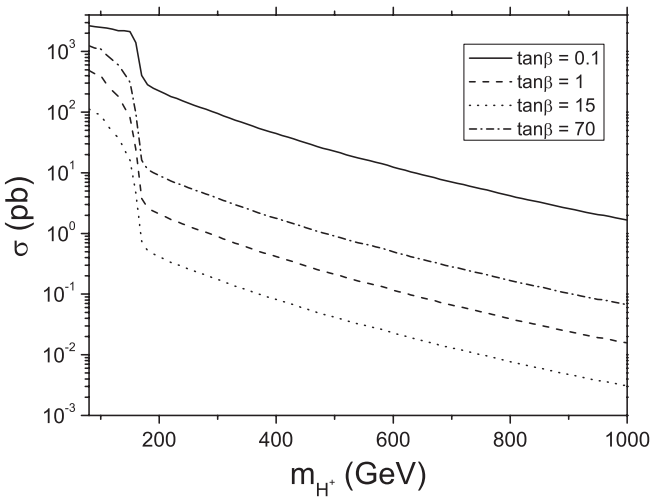

FIG. 18. The same as in Fig. 15 but taking $\tilde{\chi}^u_{ij} = 0.1$ and $\tilde{\chi}^d_{ij} = 0.1$ (scenario D).

V. EVENT RATES OF CHARGED HIGGS BOSONS AT THE LHC

To illustrate the type of charged Higgs signatures that have the potential to be detectable at the LHC in the 2HDM-III, we show in Tables I and II the event rates of a charged Higgs boson through the channels $q\bar{q}, gg \to t\bar{b}H_i^- + \text{c.c.}$ and $c\bar{b} \to H^+ + \text{c.c.}$, alongside the corresponding production cross sections (σ's) and relevant BRs, for a combination of masses, $\tan\beta$, and specific 2HDM-III parameters among those used in the previous sections (assuming $m_{h^0} = 120$ GeV, $m_{A^0} = 300$ GeV, and the mixing angle at $\alpha = \pi/2$ throughout). In particular, we focus on those cases where the charged Higgs boson mass is above the threshold for $t \to bH^+$, for two reasons. On the one hand, the scope of the LHC in accessing $t \to bH^+$ decays has been established in a rather model independent way. On the other hand, we have dealt at length with the corresponding BRs in Sec. III. (As a default, we also assume an integrated luminosity of 10^5 pb^{-1}.)

To illustrate these results, let us comment on one case within each scenario. From Table I, we can see that for scenario A, with ($\tilde{\chi}^u_{ij} = 1$, $\tilde{\chi}^d_{ij} = 1$) and $\tan\beta = 15$, we have that the $H^\pm$ is heavier than $m_t - m_b$, as we take a mass $m_{H^+} = 400$, thus precluding top decay contributions, so that in this case $\sigma(pp \to t\bar{b}H^+) \approx 2.2 \times 10^{-1}$ pb, while the dominant decays are $H^+ \to t\bar{b}$, $\tau^+\nu_\tau W^+h^0$, and W^+A^0 which give a number of events of 7040, 46, 13 860, and 374, respectively. In this case the most promising signal is $H^+ \to W^+h^0$. However, when $\tan\beta = 70$ we have that all event rates increase substantially. Here the signal $H^+ \to W^+h^0$ is still the most important with an event rate of 15 480.

Then, for scenario B ($\tilde{\chi}^u_{ij} = 0.1$, $\tilde{\chi}^d_{ij} = 1$), we have that $H^\pm$ is again above the threshold for $t \to H^+b$. So, for the declared values of the relevant parameters, we take a charged Higgs boson mass $m_{H^+} = 600$ for $\tan\beta = 1$ and $\tan\beta = 70$, respectively. In such a case the decay $H^+ \to W^+h^0$ can reach significant numbers for the LHC. We obtain a number of events of 3960 and 2703, respectively. The other decay that has a large BR is $H^+ \to W^+A^0$, and in these cases the number of events ranges over 1200–3500.

Next, we discuss scenario C ($\tilde{\chi}^u_{ij} = 1$, $\tilde{\chi}^d_{ij} = 0.1$) for $\tan\beta = 15$. Here we obtain that the signals $H^+ \to t\bar{b}$ and W^+h^0 are the most relevant ones, with a number of events about 34 560 and 26 240, respectively.

Finally, for scenario D ($\tilde{\chi}^u_{ij} = 0.11$, $\tilde{\chi}^d_{ij} = 0.1$) the dominant decays are $H^+ \to t\bar{b}$, $\tau^+\nu_\tau$, and W^+h^0, which give a spectacular number of events: 269 800, 68 400, and 34 200, respectively. Here we have set $\tan\beta = 70$.

All of these rates correspond to the case of indirect production. The contribution due to direct production is in fact subleading, especially at large $m_{H^\pm}$ values. Nonetheless, in some benchmark cases, they could represent a sizable addition to the signal event rates. This is

TABLE I. Summary of LHC event rates for some parameter combinations within scenarios A–D for an integrated luminosity of 10^5 pb^{-1}, for several different signatures, through the channel $q\bar{q}, gg \to \bar{t}bH^+ + \text{c.c.}$

$(\tilde{\chi}^u_{ij}, \tilde{\chi}^d_{ij})$	$\tan\beta$	m_{H^+} in GeV	$\sigma(pp \to H^+\bar{t}b)$ in pb	Relevant BRs	No. events
(1, 1)	15	400	2.23×10^{-1}	$\mathrm{BR}(H^+ \to t\bar{b}) \approx 3.2 \times 10^{-1}$	7040
				$\mathrm{BR}(H^+ \to \tau^+\nu^0_\tau) \approx 2.1 \times 10^{-3}$	46
				$\mathrm{BR}(H^+ \to W^+h^0) \approx 6.3 \times 10^{-1}$	13 860
				$\mathrm{BR}(H^+_2 \to W^+A^0) \approx 1.7 \times 10^{-2}$	374
(1, 1)	70	400	4.3×10^{-1}	$\mathrm{BR}(H^+ \to t\bar{b}) \approx 3.5 \times 10^{-1}$	15 050
				$\mathrm{BR}(H^+ \to c\bar{b}) \approx 1.4 \times 10^{-2}$	602
				$\mathrm{BR}(H^+ \to \tau^+\nu_\tau) \approx 2.5 \times 10^{-1}$	10 750
				$\mathrm{BR}(H^+ \to W^+h^0) \approx 3.6 \times 10^{-1}$	15 480
(0.1, 1)	1	600	1.1×10^{-1}	$\mathrm{BR}(H^+ \to t\bar{b}) \approx 3 \times 10^{-1}$	3300
				$\mathrm{BR}(H^+ \to t\bar{s}) \approx 9.1 \times 10^{-4}$	10
				$\mathrm{BR}(H^+ \to W^+h^0) \approx 3.6 \times 10^{-1}$	3960
				$\mathrm{BR}(H^+ \to W^+A^0) \approx 3.2 \times 10^{-1}$	3520
(0.1, 1)	70	600	5.1×10^{-2}	$\mathrm{BR}(H^+ \to \tau^+\nu_\tau) \approx 1.2 \times 10^{-1}$	612
				$\mathrm{BR}(H^+ \to t\bar{b}) \approx 9.4 \times 10^{-2}$	470
				$\mathrm{BR}(H^+ \to W^+h^0) \approx 5.3 \times 10^{-1}$	2703
				$\mathrm{BR}(H^+ \to W^+A^0) \approx 2.3 \times 10^{-1}$	1173
(1, 0.1)	15	300	6.4×10^{-1}	$\mathrm{BR}(H^+ \to t\bar{b}) \approx 5.4 \times 10^{-1}$	34 560
				$\mathrm{BR}(H^+ \to c\bar{b}) \approx 5 \times 10^{-4}$	32
				$\mathrm{BR}(H^+ \to \tau^+\nu_\tau) \approx 3.9 \times 10^{-2}$	2535
				$\mathrm{BR}(H^+ \to W^+h^0) \approx 4.1 \times 10^{-1}$	26 240
(0.1, 0.1)	70	300	3.8	$\mathrm{BR}(H^+ \to \tau^+\nu_\tau) \approx 1.8 \times 10^{-1}$	68 400
				$\mathrm{BR}(H^+ \to t\bar{b}) \approx 7.1 \times 10^{-1}$	269 800
				$\mathrm{BR}(H^+ \to c\bar{b}) \approx 2.4 \times 10^{-3}$	912
				$\mathrm{BR}(H^+ \to W^+h^0) \approx 9 \times 10^{-2}$	34 200

TABLE II. Summary of LHC event rates for some parameter combinations within scenarios A–D for an integrated luminosity of 10^5 pb^{-1}, for several different signatures, through the channel $c\bar{b} \to H^+ + \text{c.c.}$

$(\tilde{\chi}^u_{ij}, \tilde{\chi}^d_{ij})$	$\tan\beta$	m_{H^+} in GeV	$\sigma(pp \to H^+ + X)$ in pb	Relevant BRs	No. events
(1, 1)	15	400	1.14×10^{-1}	$\mathrm{BR}(H^+ \to t\bar{b}) \approx 3.2 \times 10^{-1}$	3648
				$\mathrm{BR}(H^+ \to \tau^+\nu^0_\tau) \approx 2.1 \times 10^{-3}$	24
				$\mathrm{BR}(H^+ \to W^+h^0) \approx 6.3 \times 10^{-1}$	7182
				$\mathrm{BR}(H^+_2 \to W^+A^0) \approx 1.7 \times 10^{-2}$	194
(1, 1)	70	400	1.25×10^{-1}	$\mathrm{BR}(H^+ \to t\bar{b}) \approx 3.5 \times 10^{-1}$	4375
				$\mathrm{BR}(H^+ \to c\bar{b}) \approx 1.4 \times 10^{-2}$	175
				$\mathrm{BR}(H^+ \to \tau^+\nu_\tau) \approx 2.5 \times 10^{-1}$	3125
				$\mathrm{BR}(H^+ \to W^+h^0) \approx 3.6 \times 10^{-1}$	4500
(0.1, 1)	1	600	3.41×10^{-4}	$\mathrm{BR}(H^+ \to t\bar{b}) \approx 3 \times 10^{-1}$	10
				$\mathrm{BR}(H^+ \to t\bar{s}) \approx 9.1 \times 10^{-4}$	0
				$\mathrm{BR}(H^+ \to W^+h^0) \approx 3.6 \times 10^{-1}$	12
				$\mathrm{BR}(H^+ \to W^+A^0) \approx 3.2 \times 10^{-1}$	11
(0.1, 1)	70	600	1.98×10^{-3}	$\mathrm{BR}(H^+ \to \tau^+\nu_\tau) \approx 1.2 \times 10^{-1}$	24
				$\mathrm{BR}(H^+ \to t\bar{b}) \approx 9.4 \times 10^{-2}$	19
				$\mathrm{BR}(H^+ \to W^+h^0) \approx 5.3 \times 10^{-1}$	105
				$\mathrm{BR}(H^+ \to W^+A^0) \approx 2.3 \times 10^{-1}$	45
(1, 0.1)	15	300	3.99×10^{-1}	$\mathrm{BR}(H^+ \to t\bar{b}) \approx 5.4 \times 10^{-1}$	21 546
				$\mathrm{BR}(H^+ \to c\bar{b}) \approx 5 \times 10^{-4}$	20
				$\mathrm{BR}(H^+ \to \tau^+\nu_\tau) \approx 3.9 \times 10^{-2}$	1556
				$\mathrm{BR}(H^+ \to W^+h^0) \approx 4.1 \times 10^{-1}$	16 359
(0.1, 0.1)	70	300	3.88×10^{-1}	$\mathrm{BR}(H^+ \to \tau^+\nu_\tau) \approx 1.8 \times 10^{-1}$	6984
				$\mathrm{BR}(H^+ \to t\bar{b}) \approx 7.1 \times 10^{-1}$	27 548
				$\mathrm{BR}(H^+ \to c\bar{b}) \approx 2.4 \times 10^{-3}$	93
				$\mathrm{BR}(H^+ \to W^+h^0) \approx 9 \times 10^{-2}$	3492

especially the case for scenario A with $\tan\beta = 15$ or 70 and scenario C with $\tan\beta = 15$. In general, though, also considering the absence of an accompanying trigger alongside the $H^{\pm}$, for instance, a top quark produced in $gb \to H^- t$ could help to identify the signal. Thus, we expect that the impact of $c\bar{b}$ fusion at the LHC will be more marginal than that of gg fusion for large Higgs masses, in fact, at times even smaller that the contribution from $q\bar{q}$ annihilation.

VI. CONCLUSIONS

We have discussed the implications of assuming a four-zero Yukawa texture for the properties of the charged Higgs boson, within the context of a 2HDM-III. In particular, we have presented a detailed discussion of the charged Higgs boson couplings to heavy fermions and the resulting pattern for its decays. The latter clearly reflect the different coupling structure of the 2HDM-III, e.g., with respect to the 2HDM-II, so that one has at disposal more possibilities to search for $H^{\pm}$ states at current and future colliders, ideally enabling one to distinguish between different Higgs models of EWSB. We have then concentrated our analysis to the case of the LHC and showed that the production rates of charged Higgs bosons at the LHC is sensitive to the modifications of the Higgs boson couplings. We have done so by evaluating 2HDM-III effects on the top decay $t \to bH^+$ as well as in the s-channel production of $H^{\pm}$ through $c\bar{b}$ fusion and the multibody final state induced by gg fusion and $q\bar{q}$ annihilation. Finally, we have determined the number of events for the most promising LHC signatures of a $H^{\pm}$ belonging to a 2HDM-III, for both $c\bar{b} \to H^+ + \text{c.c.}$ and $q\bar{q} \to \bar{t}bH^+ + \text{c.c.}$ scatterings (the latter affording larger rates than the former). Armed with these results, we are now in a position to carry out a detailed study of signal and background rates, in order to determine the precise detectability level of each signature. However, this is beyond the scope of present work and will be the subject of a future publication.

ACKNOWLEDGMENTS

This work was supported in part by CONACyT and SNI (México). J. H.-S. thanks, in particular, CONACyT (México) for Grant No. J50027-F and SEP (México) for Grant No. PROMEP/103.5/08/1640. R. N.-P. acknowledges the Institute of Physics BUAP for warm hospitality and also financial support by CONACyT through the program *Apoyo Complementario para la Consolidación Institucional de Grupos de Investigación (Retención)*.

[1] S. L. Glashow, Nucl. Phys. **22**, 579 (1961); S. Weinberg, Phys. Rev. Lett. **19**, 1264 (1967); A. Salam, in *Proceedings of the 8th NOBEL Symposium*, edited by N. Svartholm (Almqvist and Wiksell, Stockholm, 1968), p. 367.
[2] S. Dawson *et al.*, *The Higgs Hunter's Guide*, Frontiers in Physics Vol. 80 (Addison-Wesley, Reading, MA, 1990), 2nd ed.
[3] M. Carena *et al.* (Tevatron Higgs working group), FERMILAB Report No. FERMILAB-CONF-00-279-T; arXiv:hep-ph/0010338; C. Balazs *et al.*, Phys. Rev. D **59**, 055016 (1999).
[4] J. L. Díaz-Cruz *et al.*, Phys. Rev. Lett. **80**, 4641 (1998).
[5] J. Lorenzo Diaz Cruz, AIP Conf. Proc. **1026**, 30 (2008).
[6] A. Djouadi, Phys. Rep. **459**, 1 (2008).
[7] V. D. Barger, J. L. Hewett, and R. J. N. Phillips, Phys. Rev. D **41**, 3421 (1990).
[8] See, for instance, B. Dobrescu, Phys. Rev. D **63**, 015004 (2000); see also recent work on little Higgs models: N. Arkani-Hamed, A. G. Cohen, E. Katz, and A. E. Nelson, J. High Energy Phys. 07 (2002) 034 and for AdS/CFT Higgs models: R. Contino, Y. Nomura, and A. Pomarol, Nucl. Phys. **B671**, 148 (2003); A. Aranda, J. L. Diaz-Cruz, J. Hernandez-Sanchez, and R. Noriega-Papaqui, Phys. Lett. B **658**, 57 (2007).
[9] J. Brau *et al.* (ILC Collaboration), arXiv:0712.1950; A. Djouadi, J. Lykken, K. Monig, Y. Okada, M. J. Oreglia, and S. Yamashita, arXiv:0709.1893; T. Behnke *et al.* (ILC Collaboration), arXiv:0712.2356.
[10] G. Guignard (CLIC Study Team), CERN Report No. CERN-2000-008, 2000.
[11] S. Kanemura, S. Moretti, Y. Mukai, R. Santos, and K. Yagyu, Phys. Rev. D **79**, 055017 (2009).
[12] K. S. Babu and C. F. Kolda, Phys. Lett. B **451**, 77 (1999).
[13] J. L. Diaz-Cruz, R. Noriega-Papaqui, and A. Rosado, Phys. Rev. D **71**, 015014 (2005).
[14] H. Fritzsch and Z. Z. Xing, Phys. Lett. B **555**, 63 (2003).
[15] T. P. Cheng and M. Sher, Phys. Rev. D **35**, 3484 (1987).
[16] J. L. Diaz-Cruz, R. Noriega-Papaqui, and A. Rosado, Phys. Rev. D **69**, 095002 (2004).
[17] J. L. Díaz-Cruz and M. A. Pérez, Phys. Rev. D **33**, 273 (1986); J. Gunion, G. Kane, and J. Wudka, Nucl. Phys. **B299**, 231 (1988); A. Mendez and A. Pomarol, Nucl. Phys. **B349**, 369 (1991); E. Barradas *et al.*, Phys. Rev. D **53**, 1678 (1996); M. Capdequi Peyranere, H. E. Haber, and P. Irulegui, Phys. Rev. D **44**, 191 (1991); S. Moretti and W. J. Stirling, Phys. Lett. B **347**, 291 (1995); **366**, 451 (E) (1996); A. Djouadi, J. Kalinowski, and P. M. Zerwas, Z. Phys. C **70**, 435 (1996); S. Kanemura, Phys. Rev. D **61**, 095001 (2000); J. Hernández-Sánchez *et al.*, Phys. Rev. D **69**, 095008 (2004); E. Asakawa, S. Kanemura, and J. Kanzaki, Phys. Rev. D **75**, 075022 (2007); A. Arhrib, R. Benbrik, and M. Chabab, J. Phys. G **34**, 907 (2007); Phys. Lett. B **644**, 248 (2007).

[18] J. L. Díaz-Cruz, J. Hernández-Sánchez, and J. J. Toscano, Phys. Lett. B **512**, 339 (2001).

[19] J. L. Diaz-Cruz, J. Hernandez-Sanchez, S. Moretti, and A. Rosado, Phys. Rev. D **77**, 035007 (2008); AIP Conf. Proc. **1026**, 138 (2008).

[20] E. Barradas-Guevara, O. Félix-Beltrán, J. Hernández-Sánchez, and A. Rosado, Phys. Rev. D **71**, 073004 (2005).

[21] M. A. Pérez and A. Rosado, Phys. Rev. D **30**, 228 (1984); J. Gunion *et al.*, Nucl. Phys. **B294**, 621 (1987); J. L. Díaz-Cruz and O. A. Sampayo, Phys. Rev. D **50**, 6820 (1994); J. F. Gunion, Phys. Lett. B **322**, 125 (1994).

[22] S. Moretti and K. Odagiri, Phys. Rev. D **55**, 5627 (1997); **59**, 055008 (1999); F. Borzumati, J.-L. Kneur, and N. Polonsky, Phys. Rev. D **60**, 115011 (1999); S. Moretti and D. P. Roy, Phys. Lett. B **470**, 209 (1999); D. J. Miller, S. Moretti, D. P. Roy, and W. J. Stirling, Phys. Rev. D **61**, 055011 (2000); A. A. Barrientos Bendezu and B. A. Kniehl, Phys. Rev. D **59**, 015009 (1998); **61**, 097701 (2000); **63**, 015009 (2000); O. Brein and W. Hollik, Eur. Phys. J. C **13**, 175 (2000); O. Brein, W. Hollik, and S. Kanemura, Phys. Rev. D **63**, 095001 (2001); M. Bisset, M. Guchait, and S. Moretti, Eur. Phys. J. C **19**, 143 (2001); Z. Fei *et al.*, Phys. Rev. D **63**, 015002 (2000); A. Belyaev, D. Garcia, J. Guasch, and J. Sola, J. High Energy Phys. 06 (2002) 059; Phys. Rev. D **65**, 031701 (2002); M. Bisset, F. Moortgat, and S. Moretti, Eur. Phys. J. C **30**, 419 (2003); Q. H. Cao, S. Kanemura, and C. P. Yuan, Phys. Rev. D **69**, 075008 (2004); E. Asakawa, O. Brein, and S. Kanemura, Phys. Rev. D **72**, 055017 (2005); E. Asakawa and S. Kanemura, Phys. Lett. B **626**, 111 (2005).

[23] A. Abulencia *et al.* (CDF Collaboration), Phys. Rev. Lett. **96**, 042003 (2006).

[24] For a review see F. Borzumati and A. Djouadi, Phys. Lett. B **549**, 170 (2002); D. P. Roy, Mod. Phys. Lett. A **19**, 1813 (2004).

[25] C. Amsler *et al.* (Particle Data Group), Phys. Lett. B **667**, 1 (2008).

[26] S. Kanemura, T. Kubota, and E. Takasugi, Phys. Lett. B **313**, 155 (1993); J. Horejsi and M. Kladiva, Eur. Phys. J. C **46**, 81 (2006); A. G. Akeroyd, A. Arhrib, and E. M. Naimi, Phys. Lett. B **490**, 119 (2000).

[27] H. J. He and C. P. Yuan, Phys. Rev. Lett. **83**, 28 (1999).

[28] Y. B. Dai, C. S. Huang, J. T. Li, and W. J. Li, Phys. Rev. D **67**, 096007 (2003); Z. J. Xiao and L. P. Yao, Commun. Theor. Phys. **38**, 683 (2002); C. L. Lin, C. E. Lee, and Y. W. Yang, Phys. Rev. D **50**, 558 (1994).

[29] A. E. Carcamo, R. Martinez, and J. A. Rodriguez, Eur. Phys. J. C **50**, 935 (2007); R. A. Diaz, R. Martinez, and J. Alexis Rodriguez, arXiv:hep-ph/0103307; Phys. Rev. D **64**, 033004 (2001); **63**, 095007 (2001).

[30] B. Dudley and C. Kolda, arXiv:0901.3337.

[31] F. Borzumati and C. Greub, Phys. Rev. D **59**, 057501 (1999).

[32] Z. J. Xiao and L. Guo, Phys. Rev. D **69**, 014002 (2004).

[33] N. G. Deshpande, P. Lo, J. Trampetic, G. Eilam, and P. Singer, Phys. Rev. Lett. **59**, 183 (1987).

[34] D. Bowser-Chao, K. m. Cheung, and W. Y. Keung, Phys. Rev. D **59**, 115006 (1999).

[35] A. Wahab El Kaffas, P. Osland, and O. M. Ogreid, Phys. Rev. D **76**, 095001 (2007).

[36] G. Isidori, arXiv:0710.5377.

[37] J. L. Diaz-Cruz *et al.* (unpublished).

[38] P. H. Chankowski, M. Krawczyk, and J. Zochowski, Eur. Phys. J. C **11**, 661 (1999).

[39] J. L. Diaz-Cruz, H. J. He, and C. P. Yuan, Phys. Lett. B **530**, 179 (2002).

[40] S. Dittmaier, G. Hiller, T. Plehn, and M. Spannowsky, Phys. Rev. D **77**, 115001 (2008).

[41] J. Pumplin *et al.*, J. High Energy Phys. 07 (2002) 012; D. Stump *et al.*, J. High Energy Phys. 10 (2003) 046.

[42] M. Guchait and S. Moretti, J. High Energy Phys. 01 (2002) 001.

[43] F. Borzumati, J.-L. Kneur, and N. Polonsky, in Ref. [22].

[44] D. J. Miller, S. Moretti, D. P. Roy, and W. J. Stirling, in Ref. [22].

[45] S. Moretti and D. P. Roy, in Ref. [22].

[46] D. Cavalli *et al.*, arXiv:hep-ph/0203056.

[47] K. A. Assamagan *et al.*, in Ref. [17].

[48] J. Alwall, C. Biscarat, S. Moretti, J. Rathsman, and A. Sopczak, Eur. Phys. J. C **39S1**, 37 (2005).

[49] S. Moretti, Pramana **60**, 369 (2003).

[50] K. A. Assamagan, M. Guchait, and S. Moretti, arXiv:hep-ph/0402057.

[51] G. Abbiendi, I. G. Knowles, G. Marchesini, M. H. Seymour, L. Stanco, and B. R. Webber, Comput. Phys. Commun. **67**, 465 (1992).

[52] G. Corcella *et al.*, J. High Energy Phys. 01 (2001) 010.

[53] G. Corcella *et al.*, arXiv:hep-ph/9912396; arXiv:hep-ph/0107071; arXiv:hep-ph/0201201; arXiv:hep-ph/0210213.

[54] S. Moretti, K. Odagiri, P. Richardson, M. H. Seymour, and B. R. Webber, J. High Energy Phys. 04 (2002) 028.

[55] T. Sjöstrand, Comput. Phys. Commun. **82**, 74 (1994); T. Sjöstrand, P. Edén, C. Friberg, L. Lönnblad, G. Miu, S. Mrenna, and E. Norrbin, Comput. Phys. Commun. **135**, 238 (2001); T. Sjöstrand, L. Lönnblad, and S. Mrenna, arXiv:hep-ph/0108264; T. Sjöstrand, L. Lönnblad, S. Mrenna, and P. Skands, arXiv:hep-ph/0308153.

[56] J. Alwall and J. Rathsman, J. High Energy Phys. 12 (2004) 050.

[57] S. Moretti, J. Phys. G **28**, 2567 (2002).